Cambridge Prisms: Energy Transitions

www.cambridge.org/etr

Floating solar systems for clean energy: Addressing humidity-induced corrosions

Chada Sai Sravan[1], Anik Goswami[1], Anand Kumar[2], Krishna Kumba[1], Sanjay Bhadra[3] and Soham Ghosh[4]

[1]School of Electrical Engineering, Vellore Institute of Technology – Chennai Campus, India; [2]Department of Electrical Engineering, Nirma University, India; [3]Department of Electrical Engineering, University of Engineering and Management, India and [4]Black & Veatch Corporation, USA.

Research Article

Cite this article: Sravan CS, Goswami A, Kumar A, Kumba K, Bhadra S and Ghosh S (2026). Floating solar systems for clean energy: Addressing humidity-induced corrosions. *Cambridge Prisms: Energy Transitions*, **2**, e9, 1–18 https://doi.org/10.1017/etr.2026.10016

Received: 20 February 2026 UTC
Revised: 06 May 2026 UTC
Accepted: 18 May 2026 UTC

Keywords:
floating solar; SDG 7; performance analysis; energy efficiency; degradation

Corresponding author:
Anik Goswami;
Email: anik91_go@rediffmail.com

Abstract

Floating solar photovoltaic (FSPV) systems have become one of the solutions for sustainable energy generation, especially in the face of increasing global energy demand and the depletion of traditional fossil fuels (coal and crude oil). The use of large tracts of land is one of the main problems associated with traditional land-based photovoltaic (PV) systems, as land is sometimes scarce or uneconomical. FSPV technology overcomes this constraint by utilizing the available surface area of water bodies, thereby eliminating land acquisition problems and increasing energy generation efficiency. In floating solar systems, photovoltaic modules are mounted on floating structures on water. Water has a natural cooling effect that helps regulate the temperature of the modules, resulting in higher operational efficiency compared to ground-mounted systems. This article provides a comparative analysis of the power output of floating solar and land-based solar systems through two case studies: one without considering the effect of corrosion and another considering the effect of corrosion due to wet conditions on system performance and durability. The results show that the land-based system generates an annual alternating current energy output of 17.28 GWh without considering corrosion effects, whereas the floating solar system generates 19 GWh. With respect to water-induced corrosion, although humid conditions promote corrosion and reduce module life in the floating solar system, it still demonstrates a superior power output of 5.26% compared to the land-based model. Moreover, the floating solar plant offers significant environmental advantages, such as reducing emissions by 13,679 tCO_2 annually and saving 144,067 kL of water by lowering the evaporation rate. Thus, floating solar systems can be considered a sustainable and environmentally friendly energy source in accordance with Sustainable Development Goal 7, which aims to provide affordable, reliable, sustainable and modern energy for all.

Impact statement

This study advances the understanding of floating solar photovoltaic (FSPV) systems by addressing their performance and reliability under high-humidity conditions typical of tropical environments. Beyond energy generation, the work highlights the role of FSPV in addressing land constraints, supporting the water–energy nexus and enabling sustainable infrastructure development in ecologically sensitive regions. By integrating environmental degradation into performance assessment, the study provides insights relevant for long-term system design, policy formulation and large-scale deployment of floating solar technologies in emerging energy markets.

Introduction

Energy is an indispensable resource crucial for sustaining modern society and driving global development, making a reliable supply a pressing global challenge (Mahadevan and Asafu-Adjaye, 2007; Chen and Chen, 2011). In 2024, global electricity consumption reached 29,000 TWh (International Energy Agency, 2024), with nonrenewable sources primarily coal (36.7%) and other conventional fuels (26.3%) dominating production (IEA, 2024; Ahmed et al., 2022). Conventional energy sources, while economical, pose a major threat due to significant CO_2 emissions, which drive global warming (Farghali et al., 2023; Rad et al., 2023). The resulting adverse effects, including natural calamities, soil degradation and ecosystem imbalance, necessitate an urgent global shift toward clean, inexhaustible and sustainable energy (Awaad et al., 2020; Kumar et al., 2021; Naeem and Arfaoui, 2023). Renewable sources (solar, wind and hydro) limit greenhouse gas emissions and are essential for mitigating the degradation of life on earth (Yoro and Daramola, 2020; Olczak et al., 2021). Currently, solar power contributes only 5.3% of total energy generation (Ahmed et al., 2022; Yu et al., 2022), highlighting the vast potential for expansion.

The abundance of sunlight makes it obvious that harnessing solar power is a vital step toward renewable energy generation. The factors affecting the output of photovoltaic (PV) cells are solar irradiance, sunshine duration, angle of incidence of sunlight, PV module temperature, dust and

© The Author(s), 2026. Published by Cambridge University Press. This is an Open Access article, distributed under the terms of the Creative Commons Attribution licence (http://creativecommons.org/licenses/by/4.0), which permits unrestricted re-use, distribution and reproduction, provided the original article is properly cited.

Downloaded from https://www.cambridge.org/core. 19 Nov 2026 at 19:19:49, subject to the Cambridge Core terms of use.

dirt deposition on the panel, shading effect and inverter efficiency (Sharma et al., 2023; Yadav et al., 2025). Byrack et al. (2019) discussed the effect of temperature on the performance of PV modules. The authors found that the heat due to solar radiation is not spread evenly across the module. Cooling the PV module by passive methods like adding aluminum fins on the backside of the solar cell increases the power output by 5.5%. Adinoyi and Said (2013) studied the effect of dust deposition on solar panels. They found that the power output of the PV module is decreased by 50% when left uncleaned for over 6 months in the Gulf region, and the implementation of a solar tracker has helped to decrease the dust deposition. Similarly, Kazem et al. (2023) experimented on 100 W PV modules in Oman and found that the output decreased by 40% due to dust deposition. Shading of PV modules causes a significant loss of power output even at a very small area of shading (Trzmiel et al., 2020).

Government policies and technological advancements have been pivotal in promoting solar PV technology. Improvements in semiconductor technology have driven an exponential decrease in PV module prices and a simultaneous increase in efficiency (Babich et al., 2020). Given India's rapidly increasing energy demand and its favorable tropical location with abundant sunlight (Rauf et al., 2023; Bhattacharya et al., 2024), solar energy is a strategic resource. However, conventional land-based PV (LBPV) deployment is constrained by the scarcity and high cost of land (Goswami et al., 2019). Floating solar photovoltaic (FSPV) systems address this challenge by utilizing the surface area of water bodies like reservoirs, mitigating the land acquisition problem associated with LBPV (Goswami et al., 2019).

FSPV relies on various floater mechanisms, predominantly pontoon-based floaters made of high-density polyethylene (HDPE). HDPE is lightweight, economical and corrosion-resistant, but its structural strength is limited, making it susceptible to UV damage, biofouling and mechanical stress (Dai et al., 2020; Khan and Sahai, 2024). Alternative options include metal-based floaters, which offer superior strength but face corrosion challenges (especially in saline water) (Oliveira-Pinto and Stokkermans, 2020), and durable but heavy concrete-based floaters (Huang et al., 2023). Advanced designs, such as Swimsol (styrofoam-based for high waves) and Heliofloats (air-cushion based) (Oliveira-Pinto and Stokkermans, 2020; Djalab et al., 2024), are emerging to expand FSPV applicability to challenging marine environments.

Sukarso and Kim (2020) found that FSPVs stay cool as they are floated on water bodies, which gives an added advantage of increased power output than LBPV modules. Setting up FSPV on large water bodies ensures that there will be no shading on PV modules (Sasmanto et al., 2020). Rehman et al. (2024) performed a comparative analysis of land-based PV systems and FSPV systems in Saudi Arabia. The authors found that the FSPV system was cooler by 7.5–21.3% than the ground-based system, which enabled the FSPV system to operate with 12.2% higher efficiency. A study by Singh et al. (2024) showed that even after considering water-based degradation, FSPV system operates with 4–5% higher efficiency than a similar land-based system.

FSPV also helps to diminish the evaporation of water from water bodies and helps in water conservation, thus satisfying the aims of SDG 7. SDG 7 is one of the 17 goals established by the United Nations (UN) as part of the 2030 Agenda for Sustainable Development. SDG 7 seeks to ensure access to affordable, reliable, sustainable and clean energy for all. It focuses on expanding the proportion of renewable energy and raising energy efficiency. Realizing SDG 7 is central to clean energy generation, poverty reduction and mitigating climate change (Vidović et al., 2023; Singh et al., 2024). FSPV systems have all these advantages, which make it a viable choice for renewable energy generation as it complies with the aims of SDG 7.

Despite all the advantages, FSPV systems are uniquely susceptible to water-borne degradation mechanisms, including physical, chemical and biological stressors that differ from those affecting ground-mounted panels (Liu et al., 2024). A primary concern is humidity-induced degradation, as continuous high ambient moisture exposure allows water vapor to penetrate the encapsulant. This moisture ingress facilitates internal module damage, such as delamination, corrosion of metal contacts and breakdown of electrical insulation, leading to hot spots and overall efficiency loss (Naushad et al., 2025). Furthermore, the perpetual damp environment accelerates corrosion in metallic components (frames and mounting systems), sparking electrochemical oxidation (Kumar et al., 2025; Wei et al., 2025). Over time, water vapor migration through protective coatings can cause dangerous localized corrosion, particularly crevice corrosion, in low-evaporation areas like under bolts and junction boxes, which can lead to extensive, undetected structural failure (Attar et al., 2025; Saw et al., 2025). Luo et al. (2021) reported performance loss rates of ~0.5–0.7% annually for floating PV systems. However, these values were found to be comparable to nearby rooftop PV systems, suggesting that the observed degradation was not uniquely attributable to the floating environment. Similarly, Goswami and Sadhu (2021) performed an extensive study of the FSPV system and found that water-based corrosion reduced the performance of FSPV systems. This also affected the total life of the utility-based FSPV power plants. Sahu and Sudhakar (2019) found that UV and humidity corrode the floats affecting the performance of FSPV systems. Kowsar et al. (2023) assumed an annual degradation rate of 0.72% in their PVsyst-based simulation of a proposed FSPV system in Bangladesh. This value represents a modeling input rather than an experimentally measured field degradation rate. Water quality majorly affects the performance of FSPV systems. Singh and Sadhu (2024) studied FSPV systems in India and found that the FSPV system had an annual loss of energy of 4.07% due to water salinity. Dzamesi et al. (2024) studied the FSPV system at Bui Generating Station, Ghana, and found that the humidity at the FSPV site was 73% and 62% at the LBPV site.

Humidity-induced degradation extends to corrosion under insulation, where water penetrates insulated or enclosed system areas, causing hidden corrosion and creating short-circuit or fire hazards, especially in electrical connectors and junction boxes. Accelerated corrosion tests, such as those proposed by Liu et al. (2021), are essential for accurately predicting component reliability. Studies comparing degradation have shown significant differences; for example, Mannino et al. (2023) found an offshore FSPV degradation rate of 0.95% versus 3% for an onshore system, underscoring the necessity of anticorrosive coatings and superior sealing in FSPV design.

Previous research has largely considered the FSPV performance, attributing it to water corrosion and the effects of the surrounding environment. This analysis offers a different approach, where humidity is considered the main degradation cause. In contrast to previous work, the present work typically links degradation to wide water-induced phenomena and long-term corrosion signatures. Such a targeted effort promotes the predictive knowledge of the performance degradation and reliability problems of the FSPV systems. A comparative analysis between FSPV and conventional land-based PV systems is also conducted to highlight differences in efficiency, energy yield and system behavior under identical

Downloaded from https://www.cambridge.org/core. 19 Nov 2026 at 19:19:49, subject to the Cambridge Core terms of use.

environmental conditions. Furthermore, the study integrates both economic and environmental assessments to evaluate the effect of humidity on FSPV systems and the overall feasibility of FSPV deployment considering humidity-based performance degradation. This holistic approach not only fills a critical knowledge gap but also provides valuable insights for policymakers, engineers, researchers and stakeholders aiming to understand and promote the large-scale adoption of FSPV systems in real outdoor conditions.

The remaining article is structured as follows: Section "Mathematical modeling of solar module" discusses the mathematical analysis to determine the performance of the PV cells. Section "Location and meteorology" describes the site selection and the design of the FSPV system. Section "Result and discussions" covers the performance analysis of the FSPV system, including the environmental and economic analysis. The conclusion is provided in Section "Discussion."

Mathematical modeling of a solar module

A solar cell is a PN junction where electricity is produced when there is incident light on it. The basic modeling of this solar cell is represented in Figure 1 by a current source with a resistance in series (R_{se}) along with a parallel shunt resistance (R_t) (Ebhota and Tabakov, 2023). Shunt or parallel resistance basically denotes the leakage currents and other resistances. Series resistance is primarily the total resistance between the P layer and N layer of the cell; it also considers the resistances between each layer and the metal frames (Ma et al., 2019).

The output current of the solar cell (I_s), given in Eq.1, is calculated by applying Kirchhoff's current law (KCL) (Nguyen and Nguyen, 2015; Ma et al., 2019).

$$I_s = I_{sm} - I_{pn} - I_t \tag{1}$$

where I_{sm} is the photocurrent, I_{pn} is the diode current and the current through the shunt resistance is I_t. I_{pn} is the current flowing through the diode. By further substitution, I_s can be written as:

$$I_s = I_{sm} - I_{pn} - \left(\frac{V_s + I_s R_{se}}{R_t}\right) \tag{2}$$

Applying the Shockley equation for the diode:

$$I_{pn} = I_{rs}\left(e^{\frac{V_s + I_s R_{se}}{nV_{th}}} - 1\right) \tag{3}$$

where I_{rs} represents the saturation current of the diode in the reverse direction. V_{th} is the thermal voltage, n is the ideality factor and V_s is the output voltage of the PV cell. I_s is the output current of the PV cell. Calculation of V_{th} is given in Eq. 4.

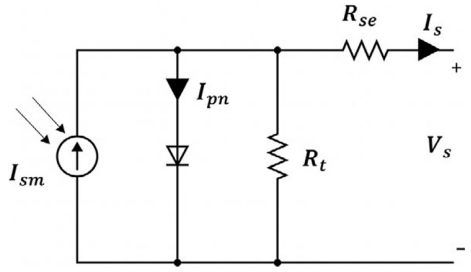


Figure 1. PV cell structure.

$$V_{th} = \frac{xKT}{q} \tag{4}$$

where x represents the number of series-connected cells, K is the Boltzmann constant 1.380649×10^{-23} J/K, $q = 1.602 \times 10^{-19}$ C (charge on an electron) and T is the kelvin temperature, which is the operating temperature of the solar cell.

Combining Eqs. (2) and (3), Eq. 5 is derived as:

$$I_s = I_{sm} - I_{rs}\left(e^{\frac{V_s + I_s R_{se}}{nV_{th}}} - 1\right) - \left(\frac{V_s + I_s R_{se}}{R_t}\right) \tag{5}$$

At maximum power output, the output current (I_s) and voltage (V_s) of the solar cell become maximum.

$$I_{ms} = I_{sm} - I_{rs}\left(e^{\frac{V_m + I_m R_{se}}{nV_{th}}} - 1\right) - \left(\frac{V_m + I_m R_{se}}{R_t}\right) \tag{6}$$

where I_{ms} is the maximum output current of the PV cell and V_m is the maximum output voltage of the PV cell.

The parameters for the single diode model are determined by solving Eqs. (1–5), by taking short circuit (SC), open circuit (OC) and standard test conditions (STC) on Eq. (6).

The Eqs. (7–11) describe the temperature dependence and global irradiance dependence of the output efficiency of the device (Prakash and Singh, 2016; Goswami and Sadhu, 2022).

$$V_s(T_i, G) = V_s + C_v(T_i - T_{STC}) \tag{7}$$

Eq. 7 represents the variation of the output voltage of the solar module with temperature. Here, $V_s(T_i, G)$ is the voltage at an operating cell temperature T_i and irradiance G, while V_s is the output voltage at STC, typically defined as 25 °C and 1000 W/m^2 irradiance. C_v denotes the temperature coefficient of voltage, which is generally negative for crystalline silicon modules, indicating that voltage decreases with increasing temperature. T_{STC} is the reference temperature at STC. This linear relation shows that as the cell temperature rises above STC, the output voltage drops due to the negative temperature coefficient. Conversely, a lower operating temperature leads to a slight increase in voltage.

$$I_s(T_i, G) = I_s\frac{G}{G_{STC}} + C_i(T_i - T_{STC}) \tag{8}$$

Eq. 8 presents the variation of the output current of the solar module with temperature and irradiance. The term $I_s(T_i, G)$ accounts for the direct proportionality between current and solar irradiance, while $C_i(T_i - T_{STC})$ captures the small increase in current with rising temperature, governed by the temperature coefficient C_i. This model is essential in photovoltaic performance analysis, particularly under real-world conditions where irradiance and temperature deviate from standard test conditions.

$$V_m(T_i, G) = V_m + C_v(T_i - T_{STC}) \tag{9}$$

The variation of the maximum voltage of the solar module with temperature is given in Eq. 9

$$I_{ms}(T_i, G) = I_{ms}\frac{G}{G_{STC}} + C_i(T_i - T_{STC}) \tag{10}$$

Eq. 10 presents the effect of temperature and irradiance on the maximum current of the solar module.

$$P_{ms}(T_i, G) = V_m(T_i, G) \times I_{ms}(T_i, G) \tag{11}$$

Downloaded from https://www.cambridge.org/core. 19 Nov 2026 at 19:19:49, subject to the Cambridge Core terms of use.

Eq. 11 defines the maximum power output of a solar module as the product of voltage and current at the maximum power point (MPP), both of which depend on the operating temperature and irradiance. While voltage typically decreases with increasing temperature, current increases slightly and both increase with irradiance. This equation is fundamental in determining the real-world performance of a PV module, as it accounts for deviations from standard test conditions and reflects the actual power generation capability of the system.

Performance analysis

The power generation (P_c) of the PV system is given by Eq. 12, which is defined in terms of the conversion of incident solar irradiation into electricity.

$$P_c = \mathcal{E} \times G \times A_{real} \tag{12}$$

Here, $\mathcal{E}$ is the efficiency of the array of solar modules, A_{real} is the useful module area in m^2 and G is the solar irradiation in Watts/m^2. Eq. 12 is an ideal case scenario where there are no losses in the network. During the conversion of DC to AC, there are losses in the inverter, which reduce the output. Further considering the effect of solar module temperature (T_m), a more applicable expression of the output power for the PV system is given by

$$P_s = n\mathcal{E}_s\mathcal{E}_{inv}A_m G\left(1 - \Theta_p[T_m - T_{STC}]\right) \tag{13}$$

Here, n is the number of solar modules. $\mathcal{E}_s$ is the rated solar module efficiency and $\mathcal{E}_{inv}$ is the rated efficiency of the inverter. The area of a single module is denoted by A_m expressed in m^2. G is solar irradiation. T_m is the temperature of the module, and T_{STC} is the standard temperature condition. Θ_p is the temperature coefficient of power.

The energy yield (Y_E) is expressed as the ratio of the FSPV plant's energy output by the installed capacity of PV modules. It refers to the estimation of the actual amount of electrical energy a solar PV system can generate over a specific period under real environmental conditions, such as irradiance and temperature.

$$Y_E = \frac{E_A}{P_{cap}} \tag{14}$$

where E_A is the electricity generation in 1 year expressed in kWh and P_{cap} is the installed capacity in kW.

The performance ratio (PR) is given by

$$PR = \frac{Y_{fi}}{Y_{ref}} \tag{15}$$

PR is a key metric used to evaluate the efficiency and quality of a PV system by comparing its actual output to its theoretical maximum output under ideal conditions.

Here, Y_{fi} is the final yield and Y_{ref} is the reference yield.

The final yield Y_{fi} is defined as the ratio of total AC energy output (E_{ac}) in kWh by the PV system's maximum rating P_c in kW.

$$Y_{fi} = \frac{E_{ac}}{P_c} \tag{16}$$

The reference yield (Y_{ref}) is determined by dividing the incident solar irradiance on the solar panel in kWh/m^2 by the solar irradiance at STC in kW/m^2.

$$Y_{ref} = \frac{E_L}{G_{STC}} \tag{17}$$

The capacity utilization factor (CUF) is given by

$$CUF = \frac{E_{TA}}{365 \times P_c \times 24} \times 100 \tag{18}$$

CUF is a key performance metric that indicates how effectively a solar PV system operates over time compared to its maximum possible output under ideal conditions.

E_{TA} is the total energy in MWh supplied by the FSPV plant in 1year and the installed PV capacity is denoted by P_c in MW.

Location and meteorology

Site selection

The Northeastern region of India faces a demand–supply deficit of 5.69% in electricity (Sonowal, 2025), highlighting the need for clean and sustainable power generation solutions. Loktak Lake, located in Moirang, Manipur (24°33′ N, 93°47′ E), is the largest freshwater lake in northeastern India, covering an average area of 287 km^2 with a mean depth of 2.7 m and a pH ranging from 6.15 to 7.66. Its size varies seasonally between 250 and 500 km^2, with a catchment area of about 980 km^2.

Figures 2–5 represent the annual average data of GHI, temperature, wind speed and relative humidity, respectively, for Loktak Lake in the year 2023. The satellite weather data are taken from the National Solar Radiation Database (National Renewable Energy Laboratory, 2023) and the analysis is performed in SAM.

Loktak Lake exhibits a warm and humid climate favorable for FSPV deployment (Table 1). The average annual temperature is 28.19 °C, with a peak of about 31.5 °C in June and a minimum of 20.8 °C in January. The site records an annual mean relative humidity of 76.65% and an average wind speed of 0.2348 m/s, with the maximum in January. The average annual GHI is 192.75 W/m^2, peaking in April before gradually declining through August. The cooler lake surface also helps lower module operating temperatures

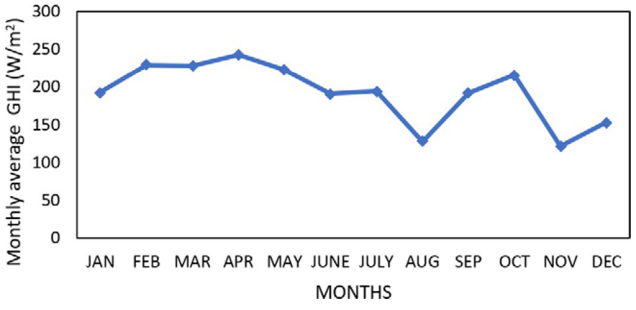


Figure 2. Monthly average GHI of Loktak Lake for the year 2023.

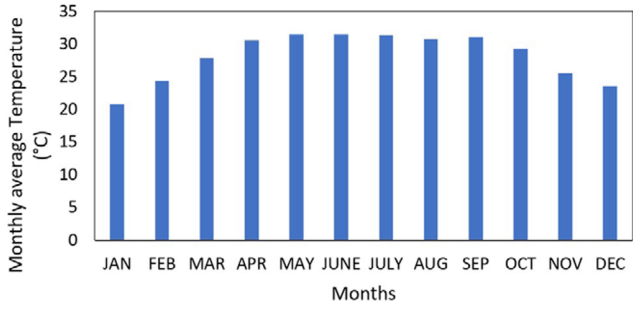


Figure 3. Monthly average temperature of Loktak Lake for the year 2023.

Downloaded from https://www.cambridge.org/core. 19 Nov 2026 at 19:19:49, subject to the Cambridge Core terms of use.

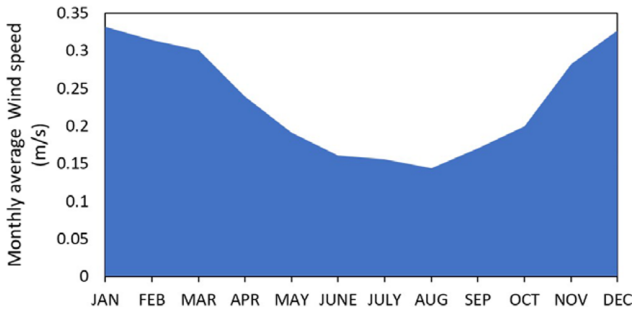


Figure 4. Monthly average wind speed of Loktak Lake for the year 2023.

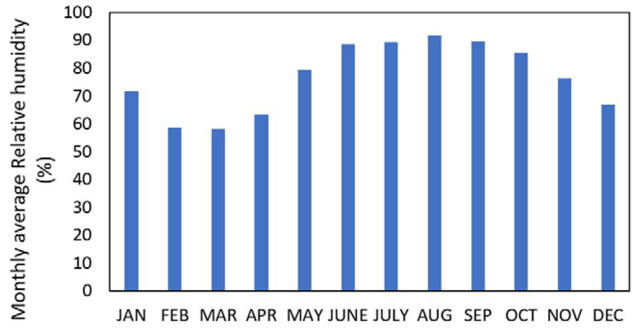


Figure 5. Monthly average relative humidity of Loktak Lake for the year 2023.

Table 1. Details of Loktak Lake (Nguyen and Nguyen, 2015)

Sl. No	Category	Descriptions
1.	District	Moirang
2.	State	Manipur
3.	Geographical coordinates	24°33′ N, 93°47′ E
4.	Mean depth	2.7 m
5.	pH range	6.15–7.66
6.	Water surface area	$287 \times 10^6\ m^2$
7.	Wind speed	2–5 km/h

by 10.8 °C, enabling higher FSPV energy yield compared to land-based systems.

Design and modeling

A 13 MW floating solar plant is designed on Loktak Lake using the software called System Advisory Model (SAM). The choice to implement the 13 MW FSPV on Loktak Lake, Manipur, was a well-weighed decision employing considerations about environmental sensitivity, technical feasibility and regional infrastructure limitations. Though the lake could easily support a much larger installation, by keeping the capacity to 13 MW, minimal disruption is caused to the ecology of diverse aquatic fauna. This capability also respects the use of the lake for fishing, along with other community uses, as it covers <1% of the water surface. The system is also appropriately sized to match regional demand and help to supply the electricity demand of Northeast India, thereby minimizing energy curtailment and ensuring efficient utilization of solar

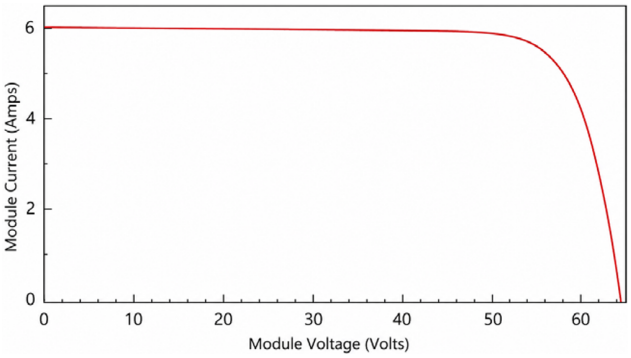


Figure 6. *I–V* characteristic graph of the solar module.

resources. Overall, the 13 MW capacity was strategically selected not as a constraint, but as a sustainable and replicable model for clean energy development in ecologically sensitive zones. The PV module used for this is SunPower's SPR-E19-310-COM. It is made up of single-crystal silicon, mono-facial. The dimensions of this module are 1.559 m in length and 1.046 m in width, making up an area of 1.631 m^2. The efficiency of this module is around 19.02%. The open circuit voltage is 64.4 V, and the short circuit current is 6A. This module provides a maximum power output of 310.149 W, with a maximum voltage of 54.7 V and a maximum current of 5.7 A. The temperature coefficient of this module is −0.386%/°C. The total number of cells used is 96. Figure 6 shows the *I–V* characteristic graph of the solar module as simulated in SAM using Eq. 8.

The inverter used for simulation is DYNAPOWER CPS-1500 Gen4 [480 V] with a maximum AC power output of 1.199 MW and a maximum DC power of 1.247 MW. The operational power used is 3922.95 Wdc. The inverter provides a nominal AC voltage of 480 V and a nominal DC voltage of 1000 V. Figure 7 shows the efficiency curve of this inverter. The minimum and maximum MPPT DC voltage are 740 V and 1500 V, respectively.

The total area covered by the modules is 68,371.520 m^2. The total number of inverters used is 13. The number of modules used is 41,920, and the number of strings is 2096. Total inverter DC capacity is 12,479,400 kW. The DC to AC ratio is kept at 1.10. Considering the civil works and overhead, the total area is taken as 83,276 m^2. The floaters used are HDPE pontoon-type floaters having a height of 0.6 m above the water surface to ensure proper

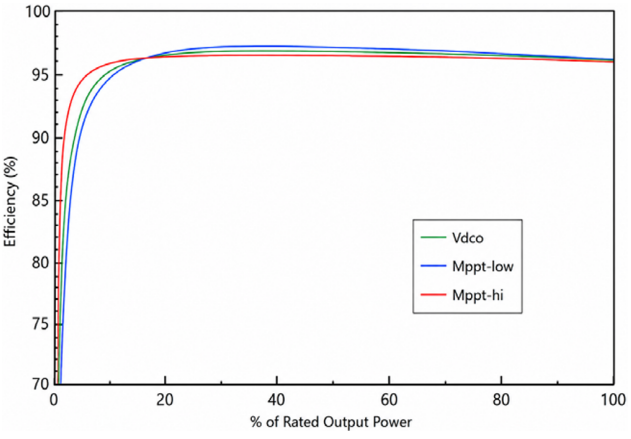


Figure 7. Efficiency curve of the inverter.

Downloaded from https://www.cambridge.org/core. 19 Nov 2026 at 19:19:49, subject to the Cambridge Core terms of use.

Table 2. Variation of energy generation with tilt angle

Sl no.	Tilt angle (degrees)	Energy (kWh/m^2)
1	0	1814
2	5	1844
3	10	1853
4	15	1864
5	20	1871
6	24	1878
7	25	1862
8	30	1835

cooling of the modules. For designing the FSPV system, when the wind speed is <7 m/s, the angle of tilt should not be <15° (Elshafei et al., 2021; National Renewable Energy Laboratory, 2023). Table 2 presents the variation of energy generated with tilt angle for the FSPV system. From Table 2, it is seen that the maximum energy generation is obtained when the tilt angle is the same as the latitude of the location. In this case, the solar panels are tilted by an angle of 24° to provide the maximum output efficiency and reduce drag force; also, the azimuth angle is 180°. The tilt angle is taken as a fixed tilt for both cases.

Generally, for areas with low wind speed, the maximum height of the wind-generated wave will be 25 cm (Elshafei et al., 2021). To decrease drag, the 13 MW FSPV system is designed to have 1 MW islands on the lake. This will guarantee that the system remains safe even during natural calamities like cyclones. This will also help to increase the reliability of the system, if any issue arises in one island, the other island will operate. The single-line diagram of the 1 MW FSPV island is given in Figure 8. The average area of the Loktak Lake is 287 km^2. Here, the FSPV system is designed with a capacity of 13 MW, having a total area of 83,276 m^2. The lake coverage by the FSPV system is 0.029% of the total lake area. The schematic diagram of the system is presented in Figure 9.

FSPV systems operate in direct contact with water and are therefore more vulnerable to environmental deterioration. Although modules, cables and inverters are designed as per IEC standards for moisture, salinity, UV exposure, humidity and mechanical stress (Dörenkämper and Arifeen Wahed, 2021), performance degradation still occurs during long-term outdoor operation. Major failures include hot spots, delamination, snail tracks, corrosion of metallic parts and biofouling from algae and aquatic organisms, all of which reduce system output (Acharya, 2022; Charles Rajesh Kumar and Majid, 2023; Cosgun and Demir, 2024). Dust accumulation and bird droppings further restrict module performance, requiring regular cleaning and preventive maintenance. Water quality also plays a significant role, and installations on freshwater bodies generally experience lower corrosion rates. Continuous inspection and maintenance are essential to ensure the reliable operation and extended lifetime of FSPV installations.

Result and discussions

The simulation of a 13 MW FSPV and LBPV power plant has been done successfully with the help of the SAM software. There are two case studies: one without considering the humidity degradation on FSPV and another case study where the humidity-based degradation is considered.

Loss consideration

Accurate loss evaluation is essential for realistic performance estimation of both LBPV and FSPV systems. Tables 3 and 4 summarize the modeled losses. Previous literature reports that module mismatch losses are around 2%, while diode and connection losses are ~0.5%. The deviation from STC is higher for LBPV (15.47%) compared to FSPV (6.998%) due to the cooling benefit of water, which reduces module operating temperature and improves efficiency (Acharya and Devraj, 2019; Kumar et al., 2021). Based on local climatic conditions, the FSPV system is expected to operate at temperatures 12.2°C lower in summer, 9.4°C in monsoon and 7.9°C in winter than LBPV modules, with the greatest benefit observed in peak summer (Haque et al., 2019; Gonzalo et al., 2020). Albedo values of 0.1 for FSPV and 0.2 for LBPV were selected based on the lower reflectivity of water surfaces (Acharya and Devraj, 2019; Mavraki et al., 2023). Although SAM simulations may deviate from real plant performance (RMSE of 0.09 for PR and 0.34 for array yield), both systems are modeled uniformly, ensuring a fair comparative analysis. For the LBPV system, the nominal DC generation is 22,415,078 kWh, and after accounting for losses (Table 3), the net delivered AC output is 17,286,254 kWh.

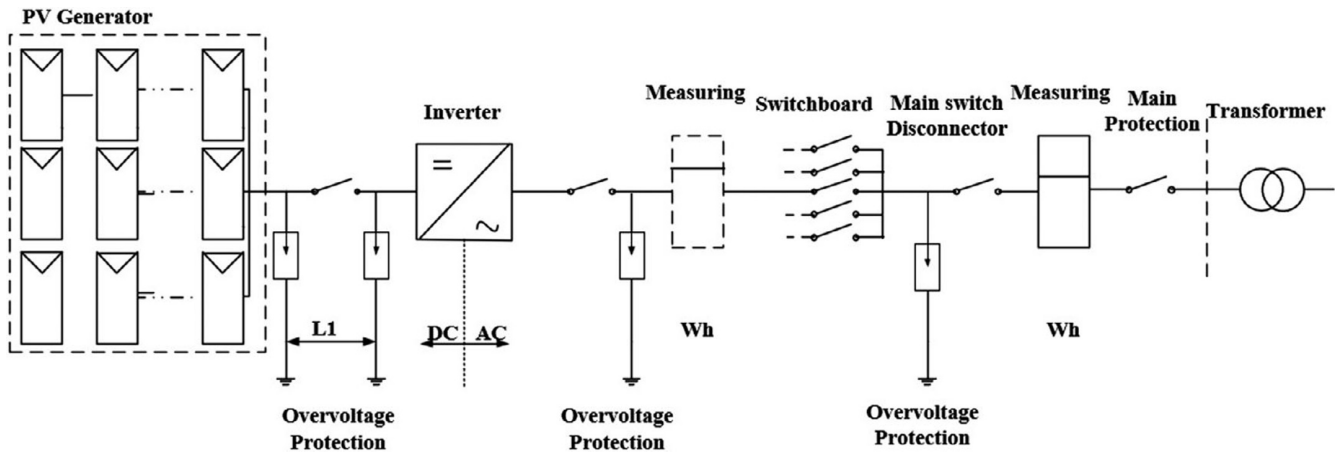


Figure 8. Schematic diagram of a 1 MW FSPV system.

Downloaded from https://www.cambridge.org/core. 19 Nov 2026 at 19:19:49, subject to the Cambridge Core terms of use.

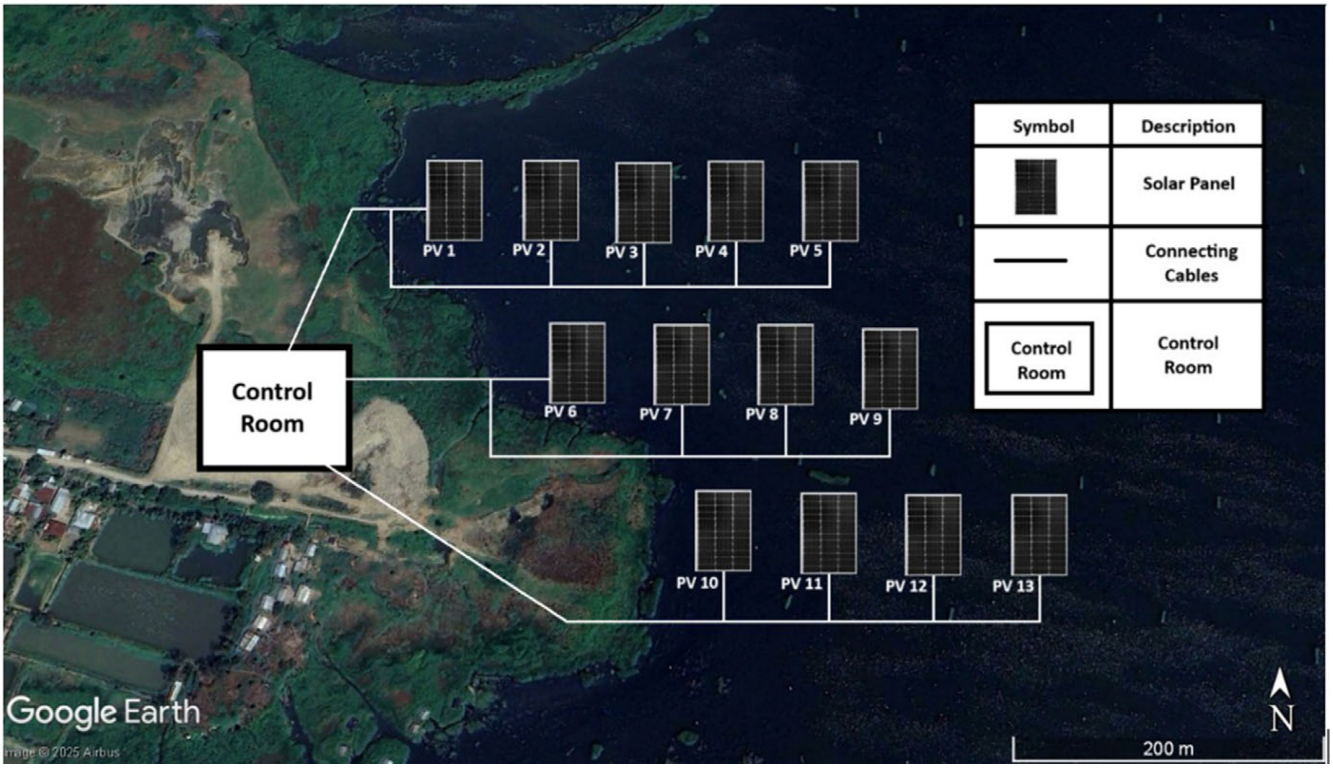


Figure 9. Schematic diagram of the FSPV system (24°33′13″ N, 93°47′56″ E) (Base image © 2025 Airbus, obtained via Google Earth Pro. Map data: Google. Image modified by the authors.).

Table 3. Losses in the LBPV system (Acharya and Devraj, 2019; Haque et al., 2019; Gonzalo et al., 2020; Kumar et al., 2021; Mavraki et al., 2023)

Sl. no.	Category	Value
1	Module mismatch	2%
2	Diodes and connections	0.5%
3	DC wiring	2%
4	Module deviation from STC	15.467%
5	Heat loss	33.5 W/m^2
6	Inverter power consumption	0.641%
7	Inverter nighttime consumption	0.108%
8	Inverter efficiency	2.835%
9	Albedo	0.2

Table 4. Losses in the FSPV system (Acharya and Devraj, 2019; Haque et al., 2019; Gonzalo et al., 2020; Kumar et al., 2021; Mavraki et al., 2023)

Sl. no.	Category	Value
1	Module mismatch	2%
2	Diodes and connections	0.5%
3	DC wiring	2%
4	Module deviation from STC	6.998%
5	Heat loss	24.6 W/m^2
6	Inverter power consumption	0.492%
7	Inverter nighttime consumption	0.098%
8	Inverter efficiency	3.054%
9	Albedo	0.1

The nominal DC electricity generation of the FSPV model is 22,415422 kWh. The losses in the FSPV system are mentioned in Table 4. The calculated net DC electricity generation is found to be 19,920,974 kWh. Considering all the losses, the net AC generation to the grid is 19,005,904 kWh.

Case 1: No degradation

The performance of the FSPV system is first evaluated under ideal operating conditions, excluding humidity-induced degradation. To establish a fair baseline, both LBPV and FSPV systems are assumed to operate at the same relative humidity (76.649%), even though FSPV systems typically experience higher moisture exposure. The monthly AC energy generation for the 1 MW systems is shown in Figure 10, calculated from the irradiance data using Eqs. 14–17.

The monthly AC energy generation data for the 1 MW LBPV system reveal distinct seasonal variations that reflect the influence of climatic and irradiance patterns across the year. The system recorded an annual energy output of 13.436 MWh, with January (1.418 MWh) and February (1.383 MWh) emerging as the most productive months, contributing ~10.33% and 10.08%, respectively, of the annual yield. These peak performances during the winter months can be attributed to clear sky conditions, lower ambient temperatures and reduced thermal losses, which typically enhance PV module efficiency. Similarly, October (1.349 MWh) also showed high output due to improved irradiance post-monsoon.

Downloaded from https://www.cambridge.org/core. 19 Nov 2026 at 19:19:49, subject to the Cambridge Core terms of use.

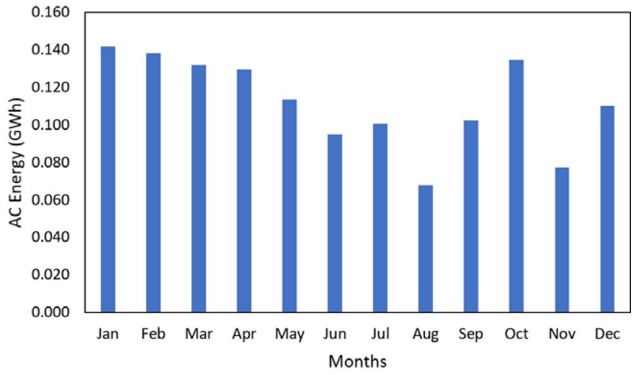


Figure 10. Monthly cumulative AC generation of 1 MW LBPV system.

In contrast, August exhibited the lowest generation (0.678 MWh), accounting for merely 4.93% of the total annual yield. This dip corresponds with the peak monsoon season in many parts of India, where dense cloud cover and reduced solar insolation significantly hinder generation. Other low-performing months include November (0.773 MWh) and June (0.951 MWh), also affected by either early monsoon conditions or reduced daylight hours. The data highlights a marked generation deficit during the monsoon period (June–August), which cumulatively contributes only 19.2% of the annual energy, underscoring the need for either complementary energy sources or improved storage solutions during this time.

On the other hand, the winter season (December–February) accounts for a surprisingly high 28.4% of the total annual generation, indicating that lower temperatures and higher solar angles contribute positively to PV performance despite shorter days. The pre-monsoon period (March–May) remains moderately productive, generating around 27.3% of the annual yield, while the post-monsoon period (September–November) contributes the remaining 22.9%. The annual AC energy generation of the 13 MW LBPV model is around 17.28 GWh. The average temperature of the LBPV modules over 1 year is around 36.12 °C, and the monthly average temperature of the LBPV modules is given in Figure 11.

The monthly performance of the 1 MW FSPV plant was analyzed using SAM, resulting in an annual energy output of 1.4708 GWh. Higher generation was recorded in January, February and October, which together contributed 29.5% of the annual output due to lower ambient temperatures and clearer sky conditions. Strong performance was also observed in March (0.1445 GWh) and April (0.1419 GWh), supported by high irradiance and moderate operating temperatures. A slight decline occurred in May (0.1247 GWh) with the onset of higher temperatures and humidity.

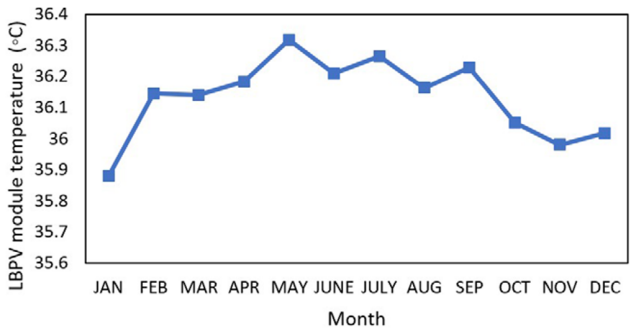


Figure 11. Temperature data of a 1 MW LPBV module.

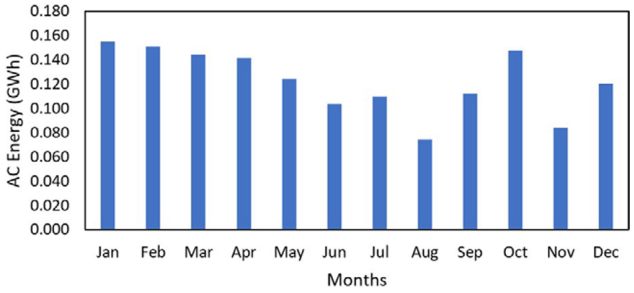


Figure 12. Monthly AC generation of a 1 MW FSPV system.

Even during the monsoon period, the system maintained stable performance, generating 0.1041 GWh in June, 0.11 GWh in July and 0.0742 GWh in August. Although output dipped in August, the reduction was less severe compared to typical land-based systems, indicating the benefits of the water-based cooling effect. Post-monsoon recovery was noticeable, with September and October producing 0.1122 and 0.1477 GWh, respectively. Moderate generation continued in November (0.0846 GWh) and December (0.1205 GWh).

Figure 12 represents the monthly AC electricity generation in year 1. The data are derived from the SAM simulations, which are calculated by Eqs. 14–17. Figure 13 shows the data of the temperature of FSPV modules, and it is observed that the average temperature is around 25.27 °C.

The output results of the 13 MW land-based solar modules and FSPV are depicted in Table 5. The annual AC energy generation of FSPV is higher than that of LBPV. The annual AC generation of FSPV is found to be 19,005,904 kWh, which is 1,719,650 kWh higher than LBPV, which generates 17,286,254 kWh. The annual performance ratio of FSPV is 17% higher than that of LBPV, which has an annual performance ratio of 72%. While the energy yield of LBPV in 1 year is 1,330 kWh/kW, the energy yield in 1 year of FSPV is found to be 1,462 kWh/kW, which is 132 kWh/kW higher.

Figure 14 shows the comparison of the net electricity generation of FSPV and land-based solar modules in 25 years of operation. It is clear that the floating solar modules produce more annual electricity than the land-based solar modules.

Case 2: Water-based degradation

The FSPV system is examined in this scenario in actual environmental conditions, paying particular attention to the impact of humidity. Due to humidity, the FSPV system undergoes degradation effecting the performance. Several studies, including IEC 61215 damp-heat qualification tests and NREL accelerated aging investigations, demonstrate that high relative humidity accelerates moisture-driven degradation mechanisms in PV modules such as metallization corrosion, EVA browning, increased series resistance and loss of fill-factor (Kempe and Wohlgemuth, 2013; Segbefia et al., 2021). However, these studies do not directly provide a closed-form equation for converting relative humidity into annual module performance loss. Therefore, in this work, a simplified and conservative humidity degradation model is introduced to translate site-specific humidity conditions into an additional degradation term and given in Eqs. 19–20 (Segbefia et al., 2021; Nobre et al., 2024).

$$Dh = \alpha(RH_{FSPV} - RH_{LBPV}) \tag{19}$$

Downloaded from https://www.cambridge.org/core. 19 Nov 2026 at 19:19:49, subject to the Cambridge Core terms of use.

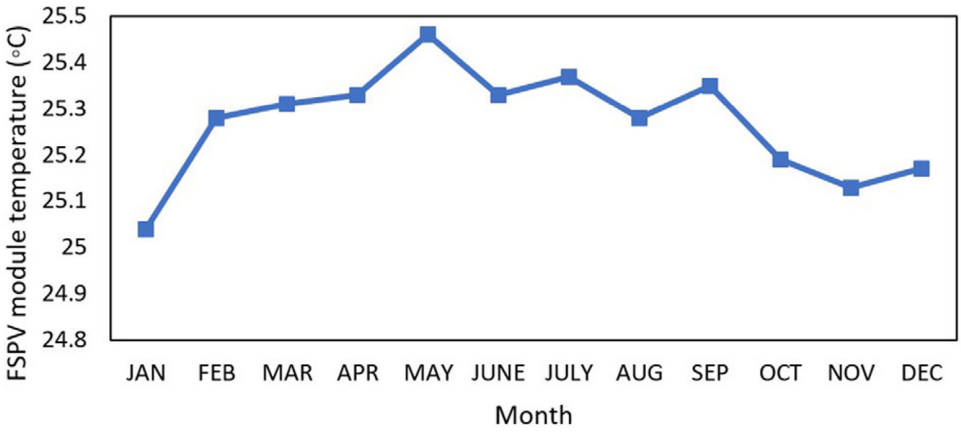


Figure 13. Temperature data of 1 MW FSPV modules.

Table 5. Performance comparison of the 13 MW LBPV and FSPV systems

Metric	LBPV value	FSPV value
Annual AC energy in Year 1	17,286,254 kWh	19,005,904 kWh
DC capacity factor in Year 1	15.20%	16.70%
Energy yield in Year 1	1,330 kWh/kW	1,462 kWh/kW
Performance ratio in Year 1	72%	89%

where RH_{FSPV} is the relative humidity of the FSPV system, RH_{LBPV} is the relative humidity of the location and α is the humidity sensitivity coefficient representing the increase in degradation per percentage point of relative humidity (RH) above the threshold.

The effective module efficiency becomes:

$$\eta_{eff} = \eta(1 - Dh) \tag{20}$$

where η is the efficiency of the system without humidity correction.

For the study location, the average relative humidity is 76.649%. Previous research has shown that FSPV systems typically experience 10–16% higher effective humidity exposure than equivalent land-based systems due to continuous proximity to the water surface and increased moisture retention (Dzamesi et al., 2024; Nobre et al., 2024; Naushad et al., 2025). In this work, the higher end of this range (14% higher RH) is adopted to evaluate a conservative worst-case scenario for the floating system, as the region is tropical and humid, and α is taken as 0.3, as per previous literature (Tripathi et al., 2021; Rajput et al., 2024). The resulting adjusted humidity value is then applied in the linear degradation formulation, providing a transparent engineering approximation for incorporating humidity-induced corrosion effects when detailed moisture-transport modeling is not available, while remaining consistent with observed performance degradation trends reported in NREL and IEC 61215 humidity–acceleration results. The humidity degradation, Dh, is applied multiplicatively to the SAM module efficiency to obtain a humidity-corrected (effective) efficiency.

It is seen that after incorporating the humidity-based degradation, the power output of FSPV is affected. Figure 15 shows the data related to the monthly AC generation of the 1 MW FSPV model in year 1 while considering humidity. The monthly values varied between 0.0689 GWh (August) and 0.1523 GWh (January). The data shows the importance of seasonal variation of humidity on the PV module performance, especially during the monsoon and post-monsoon season.

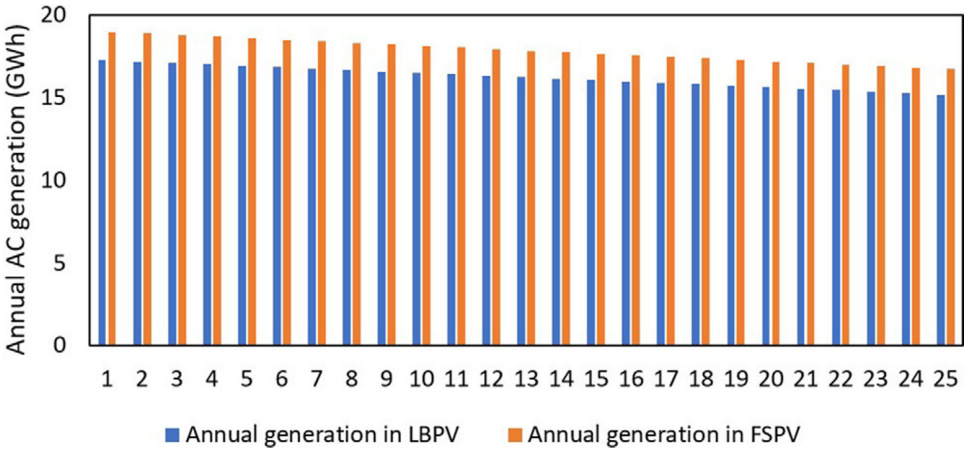


Figure 14. Comparison between 13 MW LBPV and FSPV annual AC generation.

Downloaded from https://www.cambridge.org/core. 19 Nov 2026 at 19:19:49, subject to the Cambridge Core terms of use.

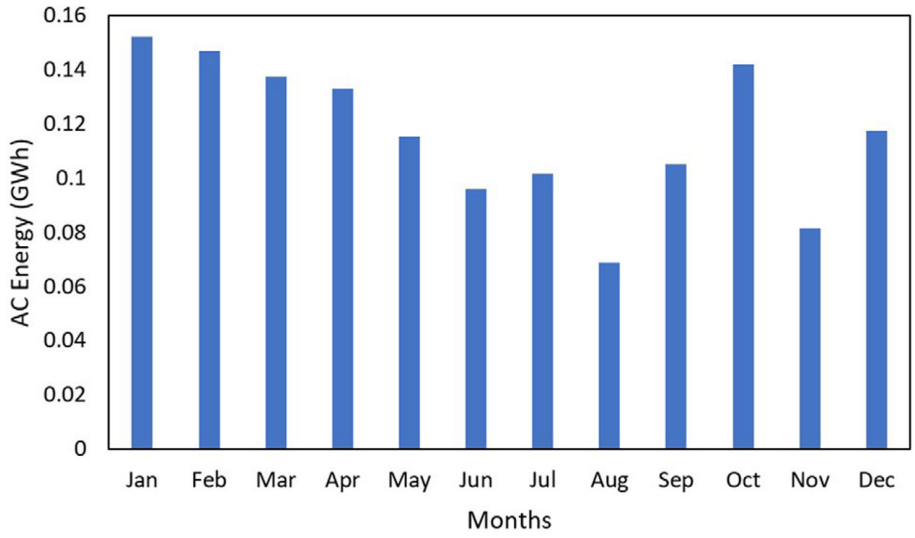


Figure 15. Monthly AC generation of 1 MW FSPV while considering humidity.

Peak generation took place in January (0.1523 GWh) and February (0.1469 GWh), representing 10.51% and 10.14%, respectively, of the annual production. These are months with clear sky, low environmental temperatures and a low level of atmospheric humidity, which contribute to the highest level of efficiency of photovoltaic conversion. Same thing for October (0.1423 GWh) and March (0.1377 GWh): the high values maintained still good performances showing that it is possible to keep the electricity performances good for moderately humid conditions when the irradiance is large enough and the thermal load is low.

The output energy reduces in the summer period (April–June) as humidity and temperature continue to rise. May (0.1154 GWh) and June (0.0962 GWh) have significantly lower than expected high generation potential, which indicates that performance starts to be impacted by rising humidity at the time. Humidity effect becomes more significant in monsoon months (July–August) with energy production decreasing to 0.1015 and 0.0689 GWh per month, respectively. The significant fall in August (providing only 4.76% of annual output) highlights the compounded effect of low solar irradiance (caused by clouds) and overcast sky.

After the monsoon, the performance starts to improve, and September (0.1054 GWh) and October (0.1423 GWh) are better. Nevertheless, residual atmospheric moisture, particularly in November (0.0815 GWh), can still influence the performance by enhancing the particulate loading and prolonging the drying time of the module surface. December (0.1177 GWh) represents a significant increase due to lower RH and a clearer sky. Notwithstanding the observed humidity-related performance losses, the FSPV system performs well compared to the LBPV system, reiterating the FSPV's viability in wet tropical environments.

In relation to its baseline 13 MW FSPV output, not including humidity (19.059 GWh), the FSPV power decrease of about 4.6% is a noticeable proof of the measurable impact of humidity on the FSPV performance, even in the case of water-cooling. This highlights the significance of incorporating one or a combination of hydrophobic coatings, an optimized cleaning regime and a passive water repellent cover to prevent moisture-related efficiency drops. Still, the FSPV system performed better than the LBPV system.

The comparison between the 13 MW LBPV, FSPV and FSPV while considering the effect of humidity is shown in Figure 16.

Considering the effect of humidity on the FSPV model designed earlier, the annual generation of electricity is found to be 18,192,366 kWh. Although it is less than that of the annual generation of FSPV, it still produces 5.24% higher energy than the LBPV model. Though the output of the FSPV system was higher, the variation of humidity affected the performance of the FSPV system and aided in the corrosion of the system. When calculated over a 25-year operational period, the FSPV system operating under humid conditions results in a cumulative loss of ~23% of the original performance, compared to 21.5% for the LBPV and FSPV systems considering no humidity degradation. This indicates that although the FSPV system initially generates more energy, sustained exposure to waterborne humidity and corrosion mechanisms progressively reduces its long-term advantage unless mitigation strategies, such as enhanced encapsulation, corrosion-resistant materials or improved sealing, are employed. Thus, it is seen that though the FSPV system has higher energy generation, it is also impacted by water-based degradation, which impacts the long-term performance of the system.

To further illustrate the performance differences among the three systems, an average daily power generation curve was developed by averaging the hourly output over the entire year for the LBPV, FSPV and FSPV with humidity models. This graph is included to visually demonstrate how the systems perform on an hourly basis and how their power production aligns with the regional electricity demand throughout the day. Such a comparison helps assess not only total annual energy generation but also the practicality and operational value of each system in matching real load requirements.

As shown in the Figure 17, both floating systems (FSPV and FSPV with humidity) begin generating electricity shortly after sunrise and reach peak output between 10:00 and 13:00, with the FSPV system showing the highest mid-day generation due to reduced module temperature and enhanced cooling over water. The LBPV system follows a similar profile but consistently produces lower power throughout the day. When humidity-induced degradation is considered, the FSPV with humidity curve remains higher than the LBPV model but demonstrates a clear reduction in peak and total output compared to the ideal FSPV case.

When compared against the hourly load demand characteristics of the Loktak region (Northern Regional Load Despatch Centre, 2025;

Downloaded from https://www.cambridge.org/core. 19 Nov 2026 at 19:19:49, subject to the Cambridge Core terms of use.

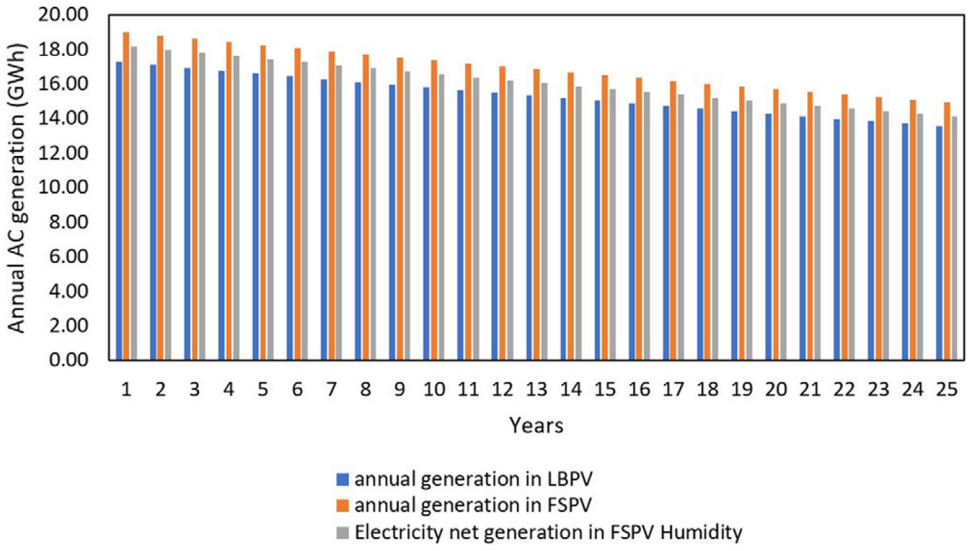


Figure 16. Annual AC electricity generation of 13 MW LBPV, FSPV and humidity considered FSPV models.

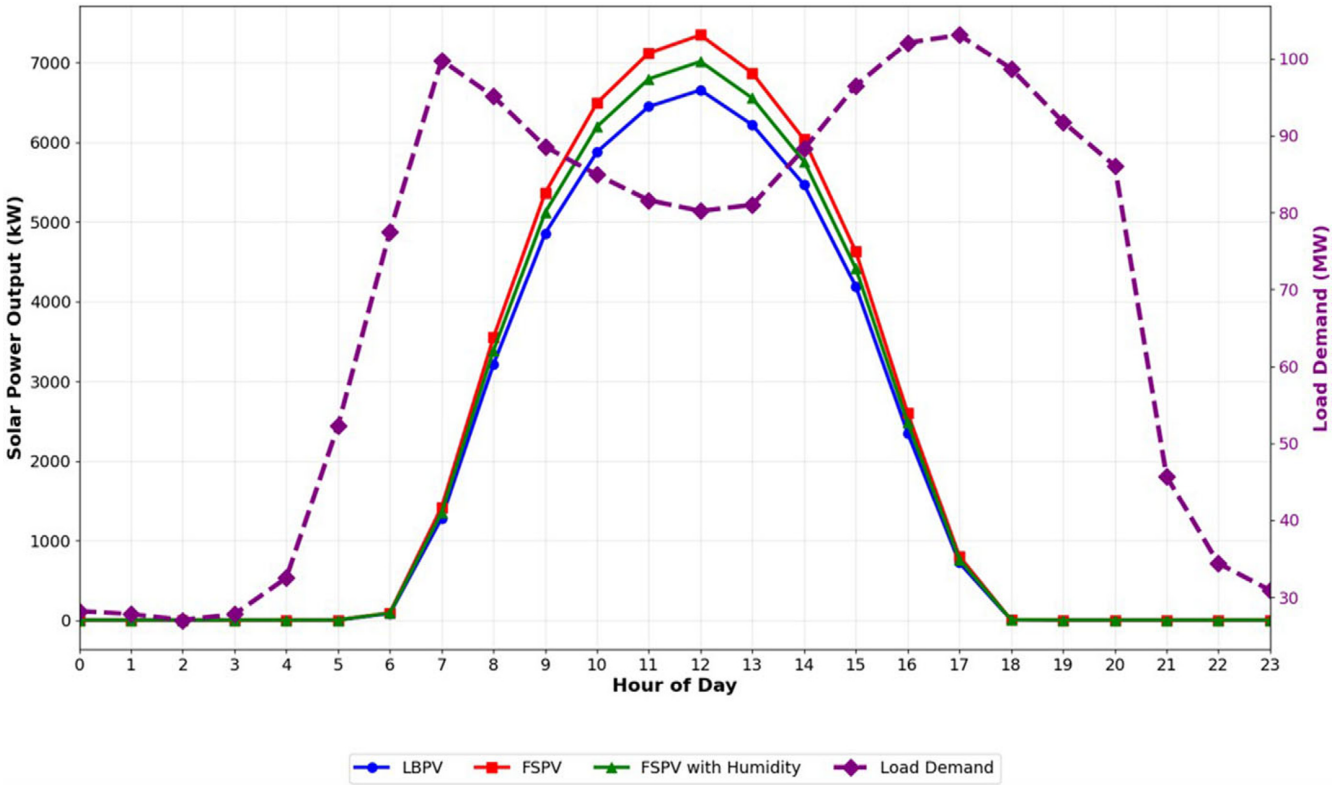


Figure 17. Daily average solar power generation and load demand of the Loktak Lake.

Northern Regional Load Despatch Centre (NERLDC), n.d.), it is evident that the highest regional electricity needs occur during the morning and evening peak periods (06:00–10:00 and 16:00–20:00), whereas PV generation peaks closer to mid-day. The results show that both floating systems (FSPV and FSPV with degradation) generate higher output from ~07:00 to 15:00 h compared to the land-based system. This advantage is due to lower module operating temperatures and better thermal conditions for water. These hours coincide with the rising daytime demand in Loktak, where the load increases sharply from around 05:00 onward. Therefore, the midday peak in FSPV generation allows a greater share of daytime demand to be met directly by solar energy, reducing grid dependence. However, during early morning and late evening hours (before 06:00 and after 17:00), PV output from all systems drops to nearly zero, while the local electricity

Downloaded from https://www.cambridge.org/core. 19 Nov 2026 at 19:19:49, subject to the Cambridge Core terms of use.

demand remains between 30 and 100 MW. This mismatch highlights the need for storage or grid support during nonsolar hours. It is important to note that the proposed 13 MW FSPV system is not intended to meet the full regional demand. Rather, the system contributes to reducing the existing demand–supply deficit, particularly during daytime hours when solar availability is highest. By delivering clean and renewable power to the grid during periods of elevated daytime demand, the FSPV installation supports improved grid stability, lowers dependence on conventional thermal generation and contributes to long-term decarbonization objectives.

Lake area coverage

For the current scenario, the lake under examination is Loktak Lake, which is the biggest freshwater lake in South Asia. The average area of the lake is 287 km^2. In this article, the FSPV system is designed with a capacity of 13 MW, having a total area of 83,276 m^2. This represents only 0.029% of the lake area. To have a better understanding of the effect of the lake coverage area on the performance of the FSPV system, the area of the lake is lowered to make it comparable with the area of the FSPV system. Hence, six cases are considered having lake coverage percentage of 10–60% and shown in Figure 18.

To evaluate the effect of lake coverage on FSPV performance, a parametric approach is adopted in which the effective coverage ratio is varied from 10 to 60%. Since the SAM does not explicitly simulate floating PV systems or coupled water–atmosphere thermal interactions, the influence of coverage is incorporated indirectly through its impact on module operating temperature. Increasing coverage reduces solar radiation incident on the water surface, which lowers the water temperature and enhances the passive cooling effect on PV modules. This reduction in module temperature is reflected in the performance model through adjusted thermal behavior, consistent with observations reported in previous FSPV studies. Therefore, the analysis captures the thermal benefits of increased coverage while maintaining a consistent simulation framework.

It is seen from Figure 18 that when the lake coverage by the FSPV module is 10%, the average power output is 15.01 GWh, and when the lake coverage is increased to 20%, the FSPV power output increases by 0.41%. Similarly, when the coverage area is increased to 30%, the power output also increases by 0.51%. This happens because with the increase in the lake coverage area, the amount of sunlight reaching the lake decreases, and the temperature of the lake is further lowered, which helps in the increment in the power output of the FSPV system, as shown in Figure 19.

When the lake coverage is more than 40%, it is observed that the power increment remains nearly constant at 0.55%, and at 60% coverage, there is a slight decrease in the power increment rate, even though the temperature is lower. This effect is interpreted as a consequence of increased module proximity and mutual shading at higher coverage levels.

In general, FSPV systems are designed such that the water coverage is no more than 25–30% of the total water surface (Benjamins et al., 2024). Higher coverage hampers the water quality as sunlight cannot reach the majority portions of the water body. This may have an adverse effect on the marine ecosystem by hampering algal growth and affecting water quality (Benjamins et al., 2024; Oliveira et al., 2024).

Environmental impact

FSPV systems also help in water conservation. FSPV systems are designed to operate on water covering the water surface, thus lowering evaporation. In India, for areas east of 85° E, the yearly evaporation loss is 1.73 kL/m^2 (Central Water Commission, 2017). The 13 MW FSPV system requires an estimated area of 83,276 m^2. The overall water savings from minimizing evaporation are 144,067 kL per year. As a result, the plant's total water usage and water required for cleaning the modules can be balanced. The FSPV system also helps to safeguard the environment by minimizing the carbon dioxide (CO_2) impact. Conventional power plants emit a significant amount of CO_2 since they utilize coal to generate electricity. In general, coal produces 0.98 kg CO_2 for every 1 kWh of energy (Rajput et al., 2020). The yearly CO_2 savings from the 13 MW FSPV plant are 13,697 tCO_2. The plant will save 342,416 tCO_2 throughout its 25-year life. All these further strengthen the FSPV system's alignment with the SDGs.

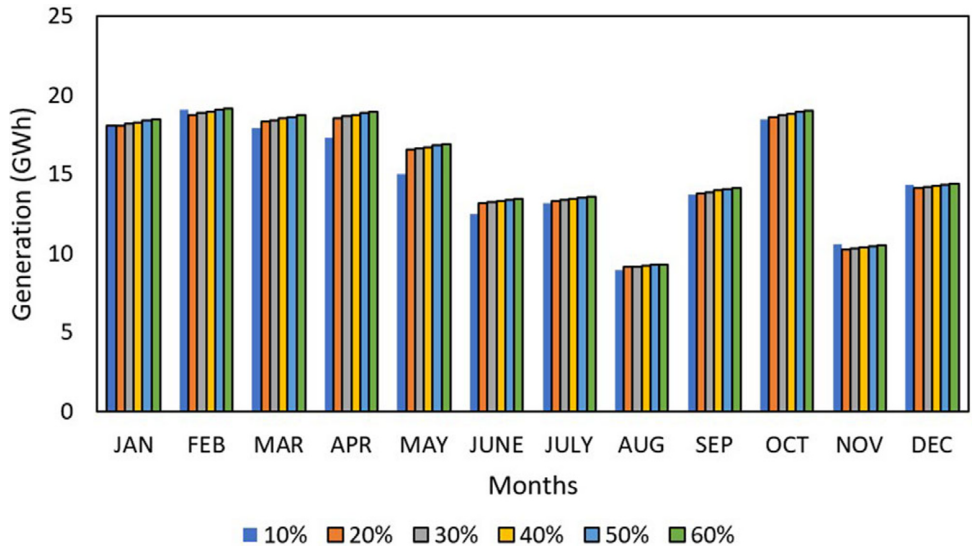


Figure 18. FSPV performance for different lake coverage.

Downloaded from https://www.cambridge.org/core. 19 Nov 2026 at 19:19:49, subject to the Cambridge Core terms of use.

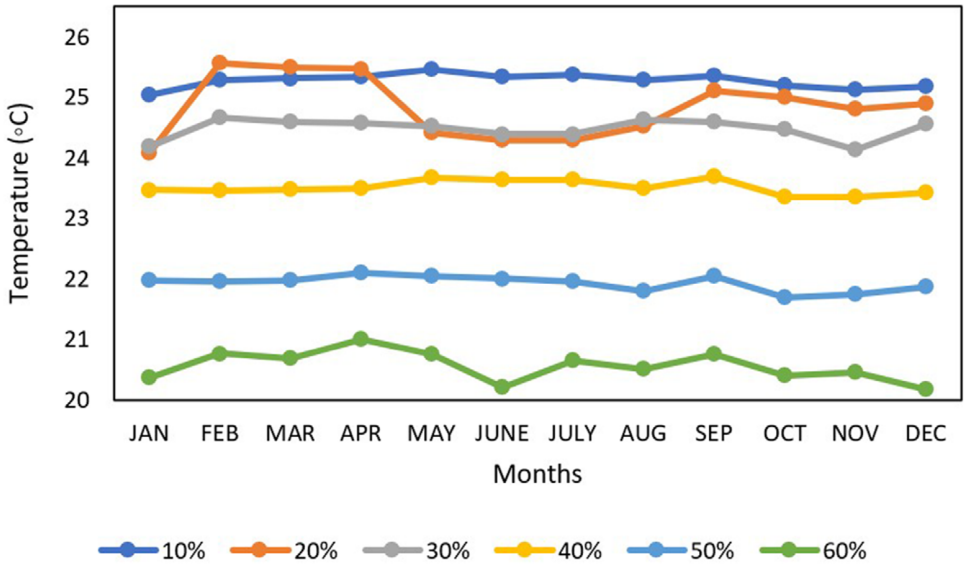


Figure 19. Temperature variation of the FSPV module with the lake coverage area.

Economic analysis

As FSPV systems are designed to work on water bodies, the cost of land is exempted from the capital cost. But FSPV systems require floaters, anchoring and mooring systems. The economic measures are computed using a variety of criteria, in compliance with the rules established by the Indian government. In the Indian scenario, the cost of land is typically taken as 0.325 $/Wp, while the cost of floaters is 0.683 $/Wp (Central Electricity Regulatory Commission, 2016; Nagananthini and Nagavinothini, 2021; Anusuya and Vijayakumar, 2024). The cost of civil works like roads, drainage and fencing is taken as 0.42 and 0.45 $/Wp for the LBPV and FSPV system, respectively. The electrical cost includes the cost of cables, junction boxes and ancillary equipment, and is taken as 0.35 $/Wp (Central Electricity Regulatory Commission, 2016; Nagananthini and Nagavinothini, 2021; Anusuya and Vijayakumar, 2024). The standard cost of setting up an LBPV system, including the land cost and module cost in India, is nearly 0.48 $/Wp. The operational cost and cost of ancillaries are higher for the FSPV system and are taken at 0.042 $/Wp, and for the LBPV system, it is 0.038 $/Wp (Anusuya and Vijayakumar, 2024; Goswami and Aizpurua, 2024). The capital cost for setting up the LBPV system is nearly 1.095 $/Wp. Considering all the economic factors, the cost of the FSPV system is 1.36 $/Wp, which is nearly 21% higher than the LBPV system. The levelized cost of electricity (LCOE) is calculated for both the FSPV and LBPV systems, considering a lifetime of 25 years. For the LCOE calculation, the discount date is taken as 8.7%, contingency as 1.5% of capital cost and inflation rate as 5.3% (da Costa and da Silva, 2021; Goswami and Aizpurua, 2024). The LCOE is calculated using Eq. 21 (da Costa and da Silva, 2021).

$$LCOE_{PV} = \left[\frac{\mathrm{CC} + \sum_{i=1}^{t} \frac{OA}{(1+DS)^i}}{\sum_{i=1}^{t} \left(\frac{E_{TA}(1-DR)^i}{(1-DS)^i}\right)}\right] \tag{21}$$

where CC represents the capital cost required to set up the system, OA is the cost required for operation, DR is the annual degradation rate and DS is the discount rate.

The payback period (PP) is the amount of time necessary for the total savings and expenses to equal or exceed the initial capital invested and is given in Eq. 22 (da Costa and da Silva, 2021).

$$PP = \frac{CC}{\sum_{i=1}^{t} C_{in}} \tag{22}$$

where cc is the total cost of the system and c_{in} is the annual cash inflow. The LCOE and payback period calculated for both the LBPV and FSPV systems are given in Table 6.

From Table 6, it is seen that the LCOE of the FSPV system is 0.0531 $, while the LCOE of the LBPV system is 0.0502 $. The LCOE of the FSPV system is 5.9% higher than the LBPV system. The LCOE of the FSPV system can be considered comparable to that of the LBPV system, as the FSPV has higher generation. Though financially LBPV systems are favorable presently, FSPV systems provide better adherence to the SDGs. With skyrocketing land prices, soon FSPV will also be a financially viable option, surpassing LBPV systems. India is a highly populated country; industrialization, along with population growth, has led to a surge in land prices. In the last 3 years, the land price in the selected location (Manipur) has risen by 4–5%. The rise in land prices is due to the increase in the state gross domestic product (SGDP). The SGDP has risen by nearly 10–11% in the last 5 years (National Bank for Agriculture and Rural Development (NABARD), 2020-21; Meitei and Sharma, 2023). With this rate, within 3–5 years the FSPV system will become a financially viable option for renewable energy generation in the Manipur area.

FSPV systems are a viable, sustainable energy alternative that supports SDG 7. Despite the initial expenditures, FSPV technology

Table 6. LCOE comparison between the LBPV and FSPV systems

Parameter	FSPV	LVPB
LCOE ($)	0.0531	0.0502
PP (years)	16.5	14.2

Downloaded from https://www.cambridge.org/core. 19 Nov 2026 at 19:19:49, subject to the Cambridge Core terms of use.

offers a revolutionary way to solar power generation that promotes innovation in renewable energy technologies. FSPV systems also support SDG 14 by reducing land-use disputes and conserving maritime environments. Overall, FPV technology is a viable option for attaining sustainable energy and green energy.

Discussion

The LBPV power plant is designed in the beginning with the help of SAM software; 17.28 GWh of energy is the annual generation of this model with a DC capacity factor of 15.2% for year 1, and energy yield in year 1 is around 1,330 kWh/kW. The total performance ratio of this model in year 1 is 72%. The major problem with the land-based PV power plant is that it requires a large area of land. India is a very population-dense country, and with the increase in population, the energy needs also increase. Keeping sustainability in mind, the motive is to go eco-friendly; thus, unconventional sources are the best way to meet these rising energy demands. With the abundance of sunlight, solar energy stands out, and in the present scenario, it is one of the major sources of renewable energy. To develop a 13 MW PV power plant, a significant area of land is required. To eliminate the land cost, the FSPV system is developed with floaters where the solar modules float on the surface of lakes, dams and so forth and such water bodies that have a larger water surface area. Therefore, a FSPV system is designed with the help of SAM software. The annual energy generation is found to be 19.05 GWh, which is 9.8% higher than the LBPV model. With a DC capacity factor of 16.7% for the year 1, 1,462 kWh/kW is the year 1 energy yield. The performance ratio of this model was 89% in year 1. The effect of humidity on FSPV is considered, and another model is designed in the SAM software. Table 7 shows the comparison between all three models.

The corrosion caused by the humidity results in degradation of the FSPV modules, which decreases the lifespan of these modules. The humidity factor causes the FSPV modules to corrode, which damages the solar modules. The power output is also affected negatively; the annual AC generation is around 18.19 GWh. The energy yield decreases for the FSPV system when humidity-based corrosion is considered. Similarly, the PR is also reduced for the FSPV system with humidity considerations due to higher losses. The energy yield refers to the actual electricity produced by that system over a given period. PR is the percentage of available energy that is actually converted into electricity, as given in Eqs. 14–17. Hence, a higher performance ratio means that a larger proportion of the available energy is used, although the total energy yield could be lower because of location and weather conditions.

However, the FSPV system still produces higher energy than that of the LBPV system even after considering the corrosion effect due to humidity. Although the FSPV model is producing higher energy, in practical applications, the humidity factor should be considered. After including the corrosion due to humidity, the FSPV model still produces significantly higher energy than that of LBPV. The FSPV system also has environmental benefits as it saves 13,679 tCO_2 and also helps to save 144,067 kL of water annually, thus aligning with the aims of SDGs.

Table 7. Comparison between the designed systems

Metric	LBPV value	FSPV value	FSPV with humidity
Annual AC energy in Year 1	17,286,254 kWh	19,005,904 kWh	18,192,366 kWh
DC capacity factor in Year 1	15.20%	16.70%	16.0%
Energy yield in Year 1	1,330 kWh/kW	1,462 kWh/kW	1,399 kWh/kW
Performance ratio in Year 1	72%	89%	76%

Conclusion

This article presents a comparative performance analysis of the performance study of 13 MW FSPV and 13 MW LBPV systems on the Loktak Lake. The novelty of this research lies in its dual-case simulation approach, which uniquely incorporates the effect of humidity-induced corrosion on FSPV performance. This article discusses two case studies: one without considering the increased humidity effect on the FSPV model and another case study where the humidity factor is considered in the FSPV model. Comparison between the LBPV model and the FSPV model (without humidity) is studied in case study 1. In the simulation of the land-based PV system, the annual AC generation was found to be 17.28 GWh. The FSPV system generates an AC energy of 19.05 GWh, which is 9.9% higher energy generation than the LBPV model. The performance ratio of the FSPV system is 89%, and the performance ratio of the LBPV system is 72%.

In case study 2, the higher corrosion due to humidity is considered in the case of the FSPV system. In the FSPV model, the solar modules are floated on the surface of the water body. It is very advantageous as the water helps cool down the surface temperature of the solar modules and increases the power output of the system. However, the humid environment also accounts for corrosion of the floater mechanism and the solar module in general, decreasing the longevity of the solar panels. More research has to be done to select proper materials for the floater mechanism, which will degrade more slowly in such a humid environment. Although humidity affects FSPV negatively, the annual power generation of FSPV is still higher than that of LBPV, with an annual AC generation of 18.19 GWh. This is 5.24% higher energy generation than the LBPV model.

FSPV is becoming increasingly competitive with land-based PV systems with advanced technologies and economic viability. The FSPV model is generating nearly 5.24% higher power output than the LBPV system, even after considering the corrosion effect on the FSPV system. The study contributes a novel methodology for evaluating long-term performance degradation due to humidity and supports global clean energy goals, particularly SDG 7, by demonstrating that FSPV systems can deliver reliable, sustainable and efficient energy in land-constrained and ecologically sensitive regions.

Nomenclature.

A. Symbols.

Table A1.

Symbol	Description
R_{se}	Resistance in series (Ω)
R_t	Shunt resistance (Ω)
I_s	The output current of the solar cell (A)
I_{sm}	Photocurrent (A)
I_t	Current through shunt resistance (a)
I_{pn}	Current though the diode (A)

(*Continued*)

Downloaded from https://www.cambridge.org/core. 19 Nov 2026 at 19:19:49, subject to the Cambridge Core terms of use.

Table A1. (*Continued*)

I_{rs}	Diode reverse saturation current (A)
V_{th}	Thermal voltage of PV cell (V)
n	Ideality factor
V_s	Output voltage of the PV cell (V)
I_s	Output current of the PV cell (A)
X	Number of series connected cells in PV module
K	Boltzmann constant (1.380649×10^{-23} J/K)
q	Charge on an electron (1.602×10^{-19} C)
T	Temperature in Kelvin
I_{ms}	Maximum output current of PV cell (A)
V_m	Maximum output voltage of the PV cell (V)
T_i	Operating cell temperature
G	Irradiance (W/m^2)
$V_s(T_i, G)$	Voltage at an operating cell temperature and irradiance (V)
C_v	Temperature coefficient of voltage
$I_s(T_i, G)$	Current at an operating cell temperature and irradiance (A)
C_i	Temperature coefficient of current
T_{STC}	Temperature at STC (K)
G_{STC}	Irradiance at STC (W/m^2)
$V_m(T_i, G)$	Maximum voltage at an operating cell temperature and irradiance (V)
$I_{ms}(T_i, G)$	Maximum current at an operating cell temperature and irradiance (A)
$P_{ms}(T_i, G)$	Maximum power output at an operating cell temperature and irradiance (W)
P_c	Power generation capacity of PV (W)
$\mathcal{E}$	Efficiency of solar modules
A_{real}	Useful module area (m^2)
P_s	Output power of solar array (W)
n	Number of solar modules
$\mathcal{E}_s$	Rated solar module efficiency
$\mathcal{E}_{inv}$	Rated efficiency of inverter
A_m	Area of single module (m^2)
T_m	Temperature of module (K)
Θ_p	Temperature coefficient of power.
Y_E	Energy yield (Wh/Wp/day)
E_A	Energy generation in one year (kWh)
P_{cap}	Installed capacity of the PV system (kW)
Y_{fi}	Final yield (kWh)
Y_{ref}	Reference yield
E_{ac}	Total AC energy output (kWh)
P_c	PV system maximum rating (kW)
E_L	Incident solar irradiance on the solar panel (kWh/m^2)
E_{TA}	Total energy supplied by the PV plant in one year (MWh)
C_{in}	Annual cash inflow

B. Abbreviations.

Table B1.

Abbreviation	Description
CC	Capital cost
CUF	Capacity utilization factor
CUI	Corrosion under insulation
DR	Degradation rate
DS	Discount rate
FSPV	Floating solar photovoltaic
GHI	Global horizontal irradiance
HDPE	High-density polyethylene
IEC	International Electrotechnical Commission
KCL	Kirchoff's current law
LBPV	Land-based photovoltaic
LCOE	Levelized cost of electricity
MPP	Maximum power point
MPPT	Maximum power point tracking
NSRDB	National solar radiation database
OA	Operational cost
OC	Open circuit
PP	Payback period
PP	Payback period
PR	Performance ratio
PV	Photovoltaic
RMSE	Root mean square error
SAM	System advisor model
SC	Short circuit
SDG	Sustainable development goal
SDM	Single diode model
SGDP	State gross domestic product
STC	Standard test conditions
UN	United Nations

Open peer review. To view the open peer review materials for this article, please visit https://doi.org/10.1017/etr.2026.10016.

Data availability statement. No primary data were generated or required for the present study. Relevant meteorological data referenced in the analysis is publicly available from the National Solar Radiation Database (NSRDB) at https://nsrdb.nrel.gov/.

Author contribution. C.S.S.: Conceptualization, methodology, data curation, software and writing – original draft preparation. A.G.: Supervision, conceptualization, writing – review and editing and corresponding author. A.K.: Methodology, validation and technical review. K.K.: Data analysis, visualization and writing – review and editing. S.B.: Corrosion assessment, environmental impact analysis and validation. S.G.: Literature review, data interpretation and writing – review and editing.

Financial support. The author did not receive any financial support.

Downloaded from https://www.cambridge.org/core. 19 Nov 2026 at 19:19:49, subject to the Cambridge Core terms of use.

Competing interests. The authors declare that they have no known competing financial interests or personal relationships that could have appeared to influence the work reported in this article.

Declaration of generative AI use in scientific writing. During the preparation of this manuscript, the author(s) utilized ChatGPT and Google Gemini to improve grammar and readability. Following the use of this tool, the author(s) carefully reviewed and revised the content as necessary and accept full responsibility for the final version of the manuscript.

References

Acharya S (2022) Analytic assessment of renewable potential in Northeast India and impact of their exploitation on environment and economy. *Environmental Science and Pollution Research* **29**(20), 29704–29718. https://doi.org/10.1007/s11356-022-18498-3.

Acharya M and Devraj S (2019) *Floating Solar Photovoltaic (FSPV): A Third Pillar to Solar PV Sector*. New Delhi: The Energy and Resources Institute.

Adinoyi MJ and Said SA (2013) Effect of dust accumulation on the power outputs of solar photovoltaic modules. *Renewable Energy* **60**, 633–636. https://doi.org/10.1016/j.renene.2013.06.014.

Ahmed A, Ge T, Peng J, Yan WC, Tee BT and You S (2022) Assessment of the renewable energy generation towards net-zero energy buildings: A review. *Energy and Buildings* **256**, 111755. https://doi.org/10.1016/j.enbuild.2021.111755.

Anusuya K and Vijayakumar K (2024) A comparative study of floating and ground-mounted photovoltaic power generation in Indian contexts. *Cleaner Energy Systems* **9**, 100140. https://doi.org/10.1016/j.cles.2024.100140.

Attar H, Alahmer A, Borowski G and Alsaqoor S (2025) Comprehensive review of advancements, challenges, design, and environmental impact in floating photovoltaic systems. *Ecological Engineering & Environmental Technology (EEET)* **26**(2), 301–322. https://doi.org/10.12912/27197050/199520.

Awaad HA, Mansour E, Akrami M, Fath HE, Javadi AA and Negm A (2020) Availability and feasibility of water desalination as a non-conventional resource for agricultural irrigation in the Mena region: A review. *Sustainability* **12**(18), 7592. https://doi.org/10.3390/su12187592.

Babich V, Lobel R and Yücel Ş (2020) Promoting solar panel investments: Feed-in-tariff vs. tax-rebate policies. *Manufacturing & Service Operations Management* **22**(6), 1148–1164. https://doi.org/10.1287/msom.2019.0860.

Bayrak F, Oztop HF and Selimefendigil F (2019) Effects of different fin parameters on temperature and efficiency for cooling of photovoltaic panels under natural convection. *Solar Energy* **188**, 484–494. https://doi.org/10.1016/j.solener.2019.06.036.

Benjamins S, Williamson B, Billing SL, Yuan Z, Collu M, Fox C, Hobbs L, Masden EA, Cottier-Cook EJ and Wilson B (2024) Potential environmental impacts of floating solar photovoltaic systems. *Renewable and Sustainable Energy Reviews* **199**, 114463. https://doi.org/10.1016/j.rser.2024.114463.

Bhattacharya S, Sadhu PK and Goswami A (2024) Energy estimation of FSPV-based microgrid for sustainable electricity generation and water conservation in hot semi-arid urban areas. *Microsystem Technologies* **30**(9), 1217–1229. https://doi.org/10.1007/s00542-024-05639-6.

Central Electricity Regulatory Commission (2016) Determination of Benchmark Capital Cost Norm for Solar PV Power Projects and Solar Thermal Power Projects Applicable During FY 2016–17. New Delhi. https://cercind.gov.in/2015/orders/SO17N.pdf (accessed on 16th September 2025).

Central Water Commission (2017) Reassessment of Water Availability in India Using Space Inputs. Basin Planning and Management Organisation. Central Water Commission, New Delhi. https://www.cwc.gov.in/en/reassessment-water-availability-india-main-report-draft (accessed on 5th September 2025)

Charles Rajesh Kumar J and Majid MA (2023) Floating solar photovoltaic plants in India–a rapid transition to a green energy market and sustainable future. *Energy & Environment* **34**(2), 304–358. https://doi.org/10.1177/0958305X211057185.

Chen ZM and Chen GQ (2011) An overview of energy consumption of the globalized world economy. *Energy Policy* **39**(10), 5920–5928. https://doi.org/10.1016/j.enpol.2011.06.046.

Cosgun AE and Demir H (2024) Investigating the effect of albedo in simulation-based floating photovoltaic system: 1 MW bifacial floating photovoltaic system design. *Energies* **17**(4), 959. https://doi.org/10.3390/en17040959.

da Costa LCA and da Silva GDP (2021) Save water and energy: A techno-economic analysis of a floating solar photovoltaic system to power a water integration project in the Brazilian semiarid. *International Journal of Energy Research* **45**(12), 17924–17941. https://doi.org/10.1002/er.6932.

Dai J, Zhang C, Lim HV, Ang KK, Qian X, Wong JLH, Tan ST and Wang CL (2020) Design and construction of floating modular photovoltaic system for water reservoirs. *Energy* **191**, 116549. https://doi.org/10.1016/j.energy.2019.116549.

Djalab A, Djalab Z, El Hammoumi A, Tina GM, Motahhir S and Laouid AA (2024) A comprehensive review of floating photovoltaic systems: Tech advances, marine environmental influences on offshore PV systems, and economic feasibility analysis. *Solar Energy* **277**, 112711. https://doi.org/10.1016/j.solener.2024.112711.

Dörenkämper M and Wahed A, Kumar A, de Jong M, Kroon J, and Reindl T (2021) "TheThe cooling effect of floating PV in two different climate zones: A comparison of field test data from the Netherlands and Singapore. *Solar Energy* **214**, 239–247. https://doi.org/10.1016/j.solener.2020.11.029.

Dzamesi SKA, Ahiataku-Togobo W, Yakubu S, Acheampong P, Kwarteng M, Samikannu R and Azeave E (2024) Comparative performance evaluation of ground-mounted and floating solar PV systems. *Energy for Sustainable Development* **80**, 101421. https://doi.org/10.1016/j.esd.2024.101421.

Ebhota WS and Tabakov PY (2023) Influence of photovoltaic cell technologies and elevated temperature on photovoltaic system performance. *Ain Shams Engineering Journal* **14**(7), 101984. https://doi.org/10.1016/j.asej.2022.101984.

Elshafei M, Ibrahim A, Helmy A, Abdallah M, Eldeib A, Badawy M and AbdelRazek S (2021) Study of massive floating solar panels over Lake Nasser. *Journal of Energy* **2021**(1), 1–17. https://doi.org/10.1155/2021/6674091.

Farghali M, Osman AI, Mohamed IM, Chen Z, Chen L, Ihara I, Yap PS and Rooney DW (2023) Strategies to save energy in the context of the energy crisis: A review. *Environmental Chemistry Letters* **21**(4), 2003–2039. https://doi.org/10.1007/s10311-023-01591-5.

Gonzalo AP, Marugán AP and Márquez FPG (2020) Survey of maintenance management for photovoltaic power systems. *Renewable and Sustainable Energy Reviews* **134**, 110347. https://doi.org/10.1016/j.rser.2020.110347.

Goswami A and Aizpurua JI (2024) Reliability-aware techno-economic assessment of floating solar power systems. *Sustainable Energy, Grids and Networks* **40**, 101536. https://doi.org/10.1016/j.segan.2024.101536.

Goswami A and Sadhu PK (2021) Degradation analysis and the impacts on feasibility study of floating solar photovoltaic systems. *Sustainable Energy, Grids and Networks* **26**, 100425. https://doi.org/10.1016/j.segan.2020.100425.

Goswami A and Sadhu PK (2022) Nature inspired evolutionary algorithm integrated performance assessment of floating solar photovoltaic module for low-carbon clean energy generation. *Sustainable Operations and Computers* **3**, 67–82. https://doi.org/10.1016/j.susoc.2021.10.002.

Goswami A, Sadhu P, Goswami U and Sadhu PK (2019) Floating solar power plant for sustainable development: A techno-economic analysis. *Environmental Progress & Sustainable Energy* **38**(6), e13268. https://doi.org/10.1002/ep.13268.

Haque A, Bharath KVS, Khan MA, Khan I and Jaffery ZA (2019) Fault diagnosis of photovoltaic modules. *Energy Science & Engineering* **7**(3), 622–644. https://doi.org/10.1002/ese3.255.

Huang G, Tang Y, Chen X, Chen M and Jiang Y (2023) A comprehensive review of floating solar plants and potentials for offshore applications. *Journal of Marine Science and Engineering* **11**(11), 2064. https://doi.org/10.3390/jmse11112064.

IEA (2024) *Global Electricity Generation by Source, 2014–2025*. International Energy Agency. Retrieved July 16, 2025, Available at https://www.iea.org/data-and-statistics/charts/global-electricity-generation-by-source-2014-2025 (accessed on 2nd August 2025).

International Energy Agency (2024) *Growth in Global Energy Demand Surged in 2024 to Almost Twice its Recent Average*. IEA. Available at https://www.iea.org/news/growth-in-global-energy-demand-surged-in-2024-to-almost-twice-its-recent-average (accessed on 2nd August 2025).

Kazem HA, Al-Waeli AH, Chaichan MT, Sopian K, Gholami A and Alnaser WE (2023) Dust and cleaning impact on the performance of photovoltaic: An

Downloaded from https://www.cambridge.org/core. 19 Nov 2026 at 19:19:49, subject to the Cambridge Core terms of use.

outdoor experimental study. *Energy Sources, Part A: Recovery, Utilization, and Environmental Effects* **45**(1), 3107–3124. https://doi.org/10.1080/15567036.2023.2191064.

Kempe MD and Wohlgemuth JH (2013) Evaluation of temperature and humidity on PV module component degradation. In *2013 IEEE 39th Photovoltaic Specialists Conference (PVSC)*. IEEE, pp. 0120–0125.

Khan MW and Sahai RSN (2024) Analysis of accelerated weathering and mechanical properties of HDPE polymer composites with carbon black and zinc oxide nanoparticles for floating solar power plants. *Journal of Renewable Energy and Environment*, **11**(3), pp. 21–34.

Kowsar A, Hassan M, Rana MT, Haque N, Faruque MH, Ahsan S and Alam F (2023) Optimization and techno-economic assessment of 50 MW floating solar power plant on Hakaluki marsh land in Bangladesh. *Renewable Energy* **216**, 119077. https://doi.org/10.1016/j.renene.2023.119077.

Kumar R, Kumar A and Pal A (2021) An overview of conventional and non-conventional hydrogen production methods. *Materials Today: Proceedings* **46**, 5353–5359. https://doi.org/10.1016/j.matpr.2020.08.793.

Kumar M, Niyaz HM and Gupta R (2021) Challenges and opportunities towards the development of floating photovoltaic systems. *Solar Energy Materials and Solar Cells* **233**, 111408. https://doi.org/10.1016/j.solmat.2021.111408.

Kumar N, Pachauri RK, Kuchhal P and Nkenyereye L (2025) Floating photovoltaic system based electrical power generation study in Indian context. *Renewable and Sustainable Energy Reviews* **212**, 115442. https://doi.org/10.1016/j.rser.2025.115442.

Liu CK, Kong ZR, Kao MJ and Wu TC (2021) A novel accelerated corrosion test for supporting devices in a floating photovoltaic system. *Applied Sciences* **11**(8), 3308. https://doi.org/10.3390/app11083308.

Liu X, Pan J, Huang H, Sun N, Gu C, Zhuang Y and Wang L (2024) Floating solar materials and their devices for energy conversion and environment remediation. *Advanced Sustainable Systems* **8**(8), 2400118. https://doi.org/10.1002/adsu.202400118.

Luo W, Isukapalli SN, Vinayagam L, Ting SA, Pravettoni M, Reindl T and Kumar A (2021) Performance loss rates of floating photovoltaic installations in the tropics. *Solar Energy* **219**, 58–64. https://doi.org/10.1016/j.solener.2020.12.019.

Ma T, Gu W, Shen L and Li M (2019) An improved and comprehensive mathematical model for solar photovoltaic modules under real operating conditions. *Solar Energy* **184**, 292–304. https://doi.org/10.1016/j.solener.2019.03.089.

Mahadevan R and Asafu-Adjaye J (2007) Energy consumption, economic growth and prices: A reassessment using panel VECM for developed and developing countries. *Energy Policy* **35**(4), 2481–2490. https://doi.org/10.1016/j.enpol.2006.08.019.

Mannino G, Tina GM, Cacciato M, Merlo L, Cucuzza AV, Bizzarri F and Canino A (2023) Photovoltaic module degradation forecast models for onshore and offshore floating systems. *Energies* **16**(5), 2117. https://doi.org/10.3390/en16052117.

Mavraki N, Bos OG, Vlaswinkel BM, Roos P, de Groot W, van der Weide B, Bittner O and Coolen JW (2023) Fouling community composition on a pilot floating solar-energy installation in the coastal Dutch North Sea. *Frontiers in Marine Science* **10**, 1223766. https://doi.org/10.3389/fmars.2023.1223766.

Meitei IL and Sharma GJ (2023) An analytical study on the inseparable relations between food, population, arable land and economy in Manipur from the perspective of sustainability. In *Sustainable Development Goals in Northeast India: Challenges and Achievements*. Singapore: Springer Nature Singapore, pp. 539–551.

Naeem MA and Arfaoui N (2023) Exploring downside risk dependence across energy markets: Electricity, conventional energy, carbon, and clean energy during episodes of market crises. *Energy Economics* **127**, 107082. https://doi.org/10.1016/j.eneco.2023.107082.

Nagananthini R and Nagavinothini R (2021) Investigation on floating photovoltaic covering system in rural Indian reservoir to minimize evaporation loss. *International Journal of Sustainable Energy* **40**(8), 781–805. https://doi.org/10.1080/14786451.2020.1870975.

National Bank for Agriculture and Rural Development (NABARD) (2020-21) *Unit Cost for Investment in Agriculture and Allied Activities – Manipur State Focus Paper, 2020–21*. Manipur Regional Office. https://www.nabard.org/info-centre-state-focus-papers.aspx?cid=512&id=698 (accessed on 1st October 2025).

National Renewable Energy Laboratory (2023) National Solar Radiation Database (NSRDB). U.S. Department of Energy. Available at https://nsrdb.nrel.gov (accessed on 17th August 2025).

Naushad NM, Rimon GR and Khan MR (2025) Local temperature and humidity aware prediction of degradation, lifetime, and long-term yield of mono-and bifacial floating photovoltaic systems. *Solar Energy* **299**, 113639. https://doi.org/10.1016/j.solener.2025.113639.

Nguyen XH and Nguyen MP (2015) Mathematical modeling of photovoltaic cell/module/arrays with tags in Matlab/Simulink. *Environmental Systems Research* **4**(1), 1–13. https://doi.org/10.1186/s40068-015-0047-9.

Nobre R, Rocha SM, Healing S, Ji Q, Boulêtreau S, Armstrong A and Cucherousset J (2024) A global study of freshwater coverage by floating photovoltaics. *Solar Energy* **267**, 112244. https://doi.org/10.1016/j.solener.2023.112244.

Northern Regional Load Despatch Centre. (2025). *Daily Load Forecast Report – Northern Region.* Available at https://www.nerldc.in/load-forecast-report-daily/ (accessed on 19th August 2025).

Northern Regional Load Despatch Centre (2026) *Day-wise Availability Schedule and Actual Generation.* Available at https://www.nerldc.in/day-wise-availability-schedule-and-actual-generation (accessed on 19th August 2025).

Olczak P, Żelazna A, Matuszewska D and Olek M (2021) The "my electricity" program as one of the ways to reduce CO2 emissions in Poland. *Energies* **14**(22), 7679. https://doi.org/10.3390/en14227679.

Oliveira PMB, Almeida RM and Cardoso SJ (2024) Effects of floating photovoltaics on aquatic organisms: A review. *Hydrobiologia* **852**, 1–16.

Oliveira-Pinto S and Stokkermans J (2020) Assessment of the potential of different floating solar technologies–overview and analysis of different case studies. *Energy Conversion and Management* **211**, 112747. https://doi.org/10.1016/j.enconman.2020.112747.

Prakash R and Singh S (2016) Designing and modelling of solar photovoltaic cell and array. *IOSR Journal of Electrical and Electronics Engineering (IOSR-JEEE)* **11**(2), 35–40.

Rad MAV, Kasaeian A, Niu X, Zhang K and Mahian O (2023) Excess electricity problem in off-grid hybrid renewable energy systems: A comprehensive review from challenges to prevalent solutions. *Renewable Energy* **212**, 538–560. https://doi.org/10.1016/j.renene.2023.05.073.

Rajput P, Malvoni M, Manoj Kumar N, Sastry OS and Jayakumar A (2020) Operational performance and degradation influenced life cycle environmental–economic metrics of mc-Si, a-Si and HIT photovoltaic arrays in hot semi-arid climates. *Sustainability* **12**(3), 1075. https://doi.org/10.3390/su12031075.

Rajput P, Singh D, Singh KY, Karthick A, Shah MA, Meena RS and Zahra MMA (2024) A comprehensive review on reliability and degradation of PV modules based on failure modes and effect analysis. *International Journal of Low-Carbon Technologies* **19**, 922–937. https://doi.org/10.1093/ijlct/ctad106.

Rauf A, Nureen N, Irfan M and Ali M (2023) The current developments and future prospects of solar photovoltaic industry in an emerging economy of India. *Environmental Science and Pollution Research* **30**(16), 46270–46281. https://doi.org/10.1007/s11356-023-25471-1.

Rehman S, Irshad K, Mohandes MA, Al-Shaikhi A and Zayed ME (2024) Comprehensive evaluation of solar floating photovoltaic prospective in Saudi Arabia: Comparative experimental investigation and thermal performance analysis. *Solar Energy* **283**, 113015. https://doi.org/10.1016/j.solener.2024.113015.

Sahu AK and Sudhakar K (2019) Effect of UV exposure on bimodal HDPE floats for floating solar application. *Journal of Materials Research and Technology* **8**(1), 147–156. https://doi.org/10.1016/j.jmrt.2017.10.002.

Sasmanto AA, Dewi T and Rusdianasari (2020) Eligibility study on floating solar panel installation over brackish water in Sungsang, South Sumatra. *EMITTER International Journal of Engineering Technology* **8**(1), 240–255. https://doi.org/10.24003/emitter.v8i1.514.

Saw MH, Heng SL, Leow SW, Nairi A and Pravettoni M (2025) Reliability of floating photovoltaics (FPV): Evaluating the effects of hydrodynamic mechanical loads on photovoltaic modules. *Japanese Journal of Applied Physics* **64**(4), 04SP50. https://doi.org/10.35848/1347-4065/adc585.

Segbefia OK, Imenes AG and Saetre TO (2021) Moisture ingress in photovoltaic modules: A review. *Solar Energy* **224**, 889–906. https://doi.org/10.1016/j.solener.2021.06.055.

Downloaded from https://www.cambridge.org/core. 19 Nov 2026 at 19:19:49, subject to the Cambridge Core terms of use.

Sharma D, **Jalil MF**, **Ansari MS and Bansal RC** (2023) A review of PV array reconfiguration techniques for maximum power extraction under partial shading conditions. *Optik* **275**, 170559. https://doi.org/10.1016/j.ijleo.2023.170559.

Singh NK and Sadhu PK (2024) The investigation of energy and economy for floating solar PV system on saline water. *Microsystem Technologies* **30**(9), 1079–1086. https://doi.org/10.1007/s00542-023-05509-7.

Singh NK, **Goswami A and Sadhu PK** (2024) Parameter extraction of floating solar PV system with war strategy optimization for sustainable cleaner generation. *Microsystem Technologies* **30**(4), 481–488. https://doi.org/10.1007/s00542-023-05555-1.

Sonowal K (2025) Changing pattern of energy usage in north East India: A historical approach. In *The Intersection of Global Energy Politics and Climate Change: A Comprehensive Analysis of Energy Markets and Economics*. Singapore: Springer Nature Singapore, pp. 167–182. https://doi.org/10.1007/978-981-96-0535-4_7.

Sukarso AP and Kim KN (2020) Cooling effect on the floating solar PV: Performance and economic analysis on the case of West Java province in Indonesia. *Energies* **13**(9), 2126. https://doi.org/10.3390/en13092126.

Tripathi AK, **Ray S**, **Aruna M and Prasad S** (2021) Evaluation of solar PV panel performance under humid atmosphere. *Materials Today: Proceedings* **45**, 5916–5920. https://doi.org/10.1016/j.matpr.2020.08.775.

Trzmiel G, **Głuchy D and Kurz D** (2020) The impact of shading on the exploitation of photovoltaic installations. *Renewable Energy* **153**, 480–498. https://doi.org/10.1016/j.renene.2020.02.010.

Vidović V, **Krajačić G**, **Matak N**, **Stunjek G and Mimica M** (2023) Review of the potentials for implementation of floating solar panels on lakes and water reservoirs. *Renewable and Sustainable Energy Reviews* **178**, 113237. https://doi.org/10.1016/j.rser.2023.113237.

Wei Y, **Khojasteh D**, **Windt C and Huang L** (2025) An interdisciplinary literature review of floating solar power plants. *Renewable and Sustainable Energy Reviews* **209**, 115094. https://doi.org/10.1016/j.rser.2024.115094.

Yadav A, **Pal N**, **Khan FA**, **Parihar RS**, **Khan A**, **Solanki S**, **Pansari D**, **Sharma P and Yadav K** (2025) Comparative assessment of various MPPT algorithms for solar photovoltaic systems under dynamic shading conditions. *Microsystem Technologies* **31**(7), 1649–1659. https://doi.org/10.1007/s00542-024-05746-4.

Yoro KO and Daramola MO (2020) CO2 emission sources, greenhouse gases, and the global warming effect. In Rahimpour MR, Farsi M, and Makarem MA (eds.), *Advances in Carbon Capture*. Woodhead Publishing, pp. 3–28. https://doi.org/10.1016/B978-0-12-819657-1.00001-3.

Yu Y, **Du E**, **Chen Z**, **Su Y**, **Zhang X**, **Yang H**, **Wang P and Zhang N** (2022) Optimal portfolio of a 100% renewable energy generation base supported by concentrating solar power. *Renewable and Sustainable Energy Reviews* **170**, 112937. https://doi.org/10.1016/j.rser.2022.112937.

Downloaded from https://www.cambridge.org/core. 19 Nov 2026 at 19:19:49, subject to the Cambridge Core terms of use.